Integrated Biomass Gasification with Catalytic Partial Oxidation for Selective Tar Conversion

Final Technical Report

Reporting Period

October 1, 2008 – February 28, 2011

Project Team:

Lingzhi Zhang, Wei Wei, Jeff Manke, Arturo Vazquez, Jeff Thompson, Mark Thompson

Fuel Conversion Laboratory
GE Global Research Center
18A Mason, Irvine, CA, 92618

Lanny Schmidt, Reetam Chakrabarti, Joshua Colby

Department of Chemical Engineering and Material Science
University of Minnesota
421 Washington Avenue SE, Minneapolis, MN 55455

May 2011

DOE Award No. DE-FG36-O8GO18085

Acknowledgment

This final technical report is based upon work supported by the Department of Energy under Award Number DE-FG36-08GO18085

Disclaimer

Table of Content

List of Figures

List of Tables

Executive Summary

Biomass gasification is a flexible and efficient way of utilizing widely available domestic renewable resources. Syngas from biomass has the potential for biofuels production, which will enhance energy security and environmental benefits. Additionally, with the successful development of low Btu fuel engines (e.g. GE Jenbacher engines), syngas from biomass can be efficiently used for power/heat co-generation. However, biomass gasification has not been widely commercialized because of a number of technical/economic issues related to gasifier design and syngas cleanup. Biomass gasification, due to its scale limitation, cannot afford to use pure oxygen as the gasification agent that used in coal gasification. Because, it uses air instead of oxygen, the biomass gasification temperature is much lower than well-understood coal gasification. The low temperature leads to a lot of tar formation and the tar can gum up the downstream equipment. Thus, the biomass gasification tar removal is a critical technology challenge for all types of biomass gasifiers. This USDA/DOE funded program (award number: DE-FG36-O8GO18085) aims to develop an advanced catalytic tar conversion system that can economically and efficiently convert tar into useful light gases (such as syngas) for downstream fuel synthesis or power generation. This program has been executed by GE Global Research in Irvine, CA, in collaboration with Professor Lanny Schmidt's group at the University of Minnesota (UoMn).

Biomass gasification produces a raw syngas stream containing H_2, CO, CO_2, H_2O, CH_4 and other hydrocarbons, tars, char, and ash. Tars are defined as organic compounds that are condensable at room temperature and are assumed to be largely aromatic. Downstream units in biomass gasification such as gas engine, turbine or fuel synthesis reactors require stringent control in syngas quality, especially tar content to avoid plugging (gum) of downstream equipment. Tar- and ash-free syngas streams are a critical requirement for commercial deployment of biomass-based power/heat co-generation and biofuels production. There are several commonly used syngas clean-up technologies: (1) Syngas cooling and water scrubbing has been commercially proven but efficiency is low and it is only effective at small scales. This route is accompanied with troublesome wastewater treatment. (2) The tar filtration method requires frequent filter replacement and solid residue treatment, leading to high operation and capital costs. (3) Thermal destruction typically operates at temperatures higher than 1000^{o}C. It has slow kinetics and potential soot formation issues. The system is expensive and materials are not reliable at high temperatures. (4) In-bed cracking catalysts show rapid deactivation, with durability to be demonstrated. (5) External catalytic cracking or steam reforming has low thermal efficiency and is faced with problematic catalyst coking.

Under this program, catalytic partial oxidation (CPO) is being evaluated for syngas tar clean-up in biomass gasification. The CPO reaction is exothermic, implying that no external heat is needed and the system is of high thermal efficiency. CPO is capable of processing large gas volume, indicating a very compact catalyst bed and a low reactor cost. Instead of traditional physical removal of tar, the CPO concept converts tar into useful light gases (eg. CO, H_2, CH_4). This eliminates waste treatment and disposal requirements. All those advantages make the CPO catalytic tar conversion system a viable solution for biomass gasification downstream gas clean-up.

This program was conducted from October 1 2008 to February 28 2011 and divided into five major tasks.

- Task A: Perform conceptual design and conduct preliminary system and economic analysis (Q1 2009 ~ Q2 2009)
- Task B: Biomass gasification tests, product characterization, and CPO tar conversion catalyst preparation. This task will be conducted after completing process design and system economics analysis. Major milestones include identification of syngas cleaning requirements for proposed system design, identification and selection of tar compounds and

mixtures for use in CPO tests, and preparation of CPO catalysts for validation. (Q3 2009 ~ Q4 2009)

- Task C: Test CPO with biomass gasification product gas. Optimize CPO performance with selected tar compounds. Optimize CPO performance with multi-component mixtures. Milestones include optimizing CPO catalysts design, collecting CPO experimental data for next stage kinetic modeling and understanding the effect of relative reactivities on ultimate tar conversion and syngas yields. (Q1 2010 ~ Q3 2010)
- Task D: Develop tar CPO kinetic model with CPO kinetic model and modeling results as deliverables. (Q3 2010 ~ Q2 2011)
- Task E: Project management and reporting. Milestone: Quarterly reports and presentations, final report, work presented at national technical conferences (Q1 2009 ~ Q2 2011)

At the beginning of the program, IP landscaping was conducted to understand the operation of various types of biomass gasifiers, their unique syngas/tar compositions and potential tar mitigation options using the catalytic partial oxidation technology. A process simulation model was developed to quantify the system performance and economics impact of CPO tar removal technology. Biomass gasification product compositions used for performance evaluation tests were identified after literature review and system modeling. A reaction system for tar conversion tests was designed, constructed, with each individual component shaken-down in 2009. In parallel, University of Minnesota built a lab-scale unit and evaluated the tar removal performance using catalytic reforming. Benzene was used as the surrogate compound. The biomass gasification raw syngas composition was provided by GE through system studies. In 2010, GE selected different tar compounds and evaluated the tar removal effectiveness of the CPO catalyst. The catalytic performance was evaluated under different operating conditions, including catalyst geometry, S/C ratio, O/C ratio, GHSV, and N_2 dilution. An understanding of how to optimize catalytic tar removal efficiency by varying operating conditions has been developed. GE collaborated with UoMn in examining inorganic impurities effects. Catalysts were pre-impregnated with inorganic impurities commonly present in biomass gasification syngas, including Si, Ca, Mg, Na, K, P and S. UoMn performed catalyst characterization and has acquired fundamental understandings of impurities effect on catalytic tar removal. Based on experimental data and the proposed reaction pathway, GE constructed a model to predict kinetic performance for biomass gasification tar cleanup process. Experimental data (eg. tar conversion, reactor inlet and outlet temperatures, product distribution) at different operating conditions were used to validate the model. A good fit between model predictions and experimental data was found. This model will be a valuable tool in designing the tar removal reactor and identifying appropriate operating conditions. We attended the 2011 DOE Biomass Program Thermochemical Platform Review held in Denver, CO from February 16 to 18 and received very positive comments from the review panel. Further, syngas utility and biomass to power/fuel companies expressed strong interest in our tar removal technology.

1. System Economic Analysis

During the early stage of the program, GE engineers conducted extensive literature reviews in order to understand the operation of various types of biomass gasifiers, their unique syngas/tar compositions and potential tar mitigation options using the catalytic partial oxidation technology. Based on this understanding, a process simulation model was developed to quantify the system performance and economics impact of CPO tar removal technology. A case study, consisting of three process configurations, was conducted and their process economics evaluated. Finally, due to the intricate relationship between power plant scale and choice of technology, we conducted a "crop-circle" based analysis to identify the optimal scale for a biomass gasification based power generation system. This analysis takes into consideration of the cost of biomass collection, transportation, gasification plant equipment cost, scale of economics, etc. and further narrows down the development and design scope of the CPO technology.

1.1 System Design

Due to the low energy content of biomass and the small-scale nature of biomass gasification operation, air blown fluidized bed gasifier is widely chosen for biomass gasification process. In addition, we believe that a chemical or thermal looping gasifier is well suited for biomass gasification operation due to the inherent separation of syngas from nitrogen and, potentially, from CO_2. Therefore, we chose these two types of gasifier as our focus for tar destruction technology development.

Typical air blown fluidized bed gasifier can produce about 1% ~ 5% tar while an indirectly heated gasifier can produce as much as 10% tar. The typical syngas composition of each of the two types of gasifier is shown in Table 1:

Type	Air FB	Indirect CFB
Fluidization Agent	steam	air
Bed Material	sand	olivine
Feed	Wood chips	Wood chips
Gas Composition		
H2	21.7	26.2
CO	23.8	38.2
CO2	9.4	15.1
N2	41.6	2
CH4	0.08	14.9
C2+	0.6	4
GCV (MJ/Nm3)	16.3	5.4

Table 1 Typical Biomass Gasification Product[1] (FB: Fluidizing Bed; CFB: Circulating Fluidized Bed)

In order to understand the tar CPO process, a system analysis model was constructed in Aspen Plus software, as shown in Figure 1. This model incorporates the biomass feeding, gasifier operations, syngas cooling, tar removal, syngas cleanup and power generations. We will use such a model to help quantify CPO reactor design criteria and perform conceptual design trade-off analysis.

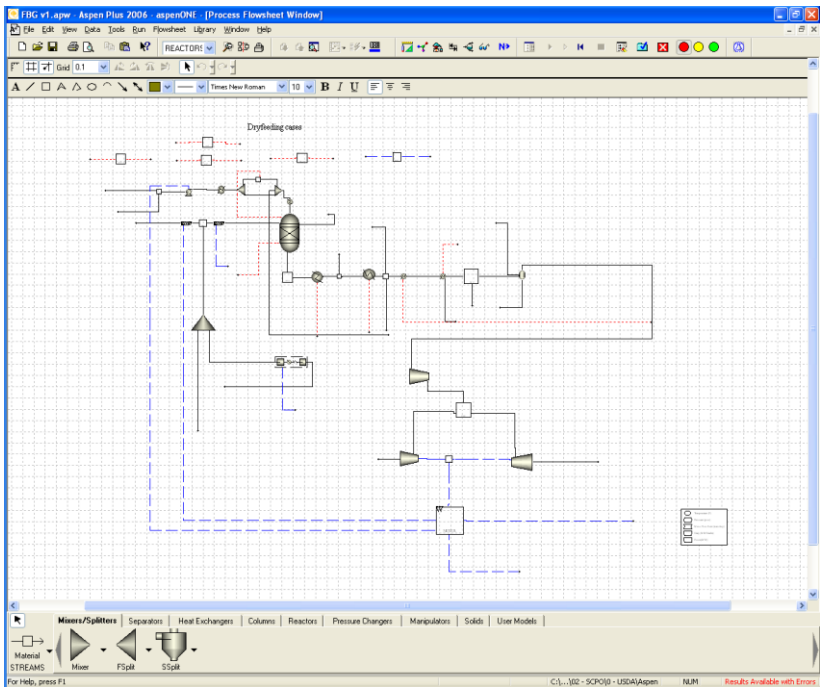

Figure 1 Biomass gasification process simulation model in AspenPlus

Table 2 shows the typical tar composition of biomass gasification and the surrogate tar composition used in Aspen system analysis.

Compound Percentage weight	Wt%
Benzene	37.9
Toluene	14.3
Other one-ring aromatic hydrocarbons	13.9
Naphthalene	9.6
Other two-ring aromatic hydrocarbons	7.8
Three-ring aromatic hydrocarbons	3.6
Four-ring aromatic hydrocarbons	0.8
Phenolic compounds	4.6
Heterocyclic compounds	6.5
Others	1

Table 2 Typical tar composition of biomass gasification[2] and surrogate tar composition

1.2 System Performance Case Study

A detailed system and economic case study was conducted to evaluate three different options for small scale power generation via biomass:

1. Low pressure fluidized biomass gasifier + wet scrubbing and filters for tar cleanup
2. Low pressure fluidized biomass gasifier + CPO for tar cleanup
3. High pressure biomass gasifier + CPO for tar cleanup

1.2.1 System descriptions

Figure 2 illustrates the process flow diagram corresponding to case 1. The typical biomass feedstock for this process includes wood chip, corn stover, grass, etc. Feedstocks are usually processed into particle size on the order of 5 mm to 20 mm and fed to the gasifier either via lock hopper or screw feeder. In this case, the gasifier operates at 2 atm and in an updraft fluidized bed mode. This type of gasifier provides excellent heat transfer in the bed and extended residence time for the feedstock, which lead to high carbon conversion efficiency of about 95%~99%[1]. Fluidized bed gasifier usually generates tar content of 1% wt of feed or about 10g/m^3. Therefore, the syngas coming out of the gasifier needs to be cleaned up for any tar or particulates prior to the IC engine for power generation. Typical cleanup processes involves wet scrubbing of the syngas and filters for particle removal.

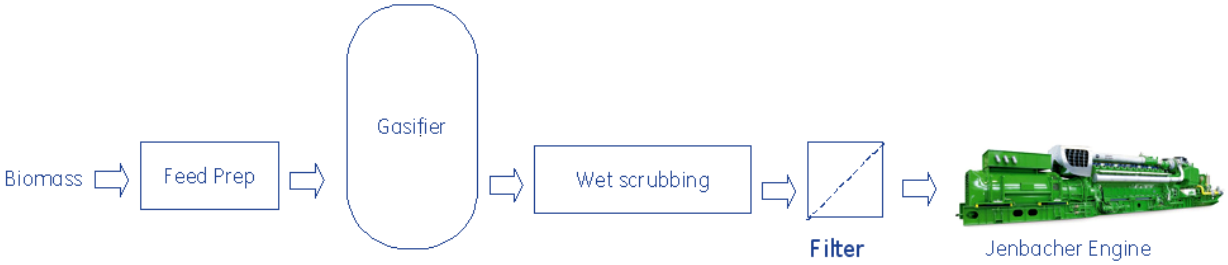

Figure 2 Process flow diagram for case 1

Figure 3 illustrates the process flow diagram corresponding to case 2. In this case, instead of using conventional wet scrubbing for tar condensation and cleanup, a catalytic partial oxidation tar cracker is used to destruct the tar in syngas. The CPO tar cracker is closely coupled with gasifier to take advantage of the high temperature of the hot syngas. No wet scrubbing is needed for this process.

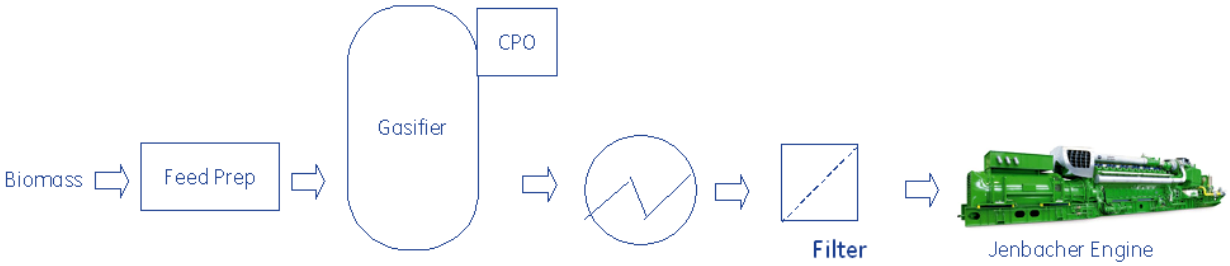

Figure 3 Process flow diagram for case 2

Figure 4 illustrates the process flow diagram corresponding to case 3. This case is similar to case 2 where a catalytic partial oxidizer bed is used to catalytically destruct tar. However, instead of operating under low pressure, this system operates at over 10~20 atm to take advantage of the equipment size reduction and to eliminate the need for fuel compressor. Traditionally, high pressure feeding into high-pressure system is accomplished via lock hopper, which can be costly and unreliable due to poor control over solid flow rates. In this case, the solid pump provides a convenient solution to the solid feeding problems.

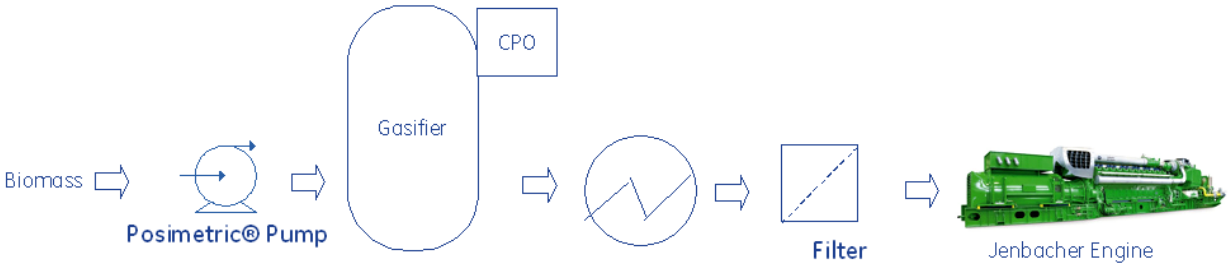

Figure 4 Process flow diagram for case 3

1.2.2 Economic analysis

Based on the configurations of these three cases, a set of Aspen models were developed to provide the process conditions and calculate energy output. We also estimated the equipment costs based on these system analysis and publicly available equipment cost estimates. The results are shown in Table 3.

Table 3 Economic analysis results

System	**Case 1: LP+WS+Filter**	**Case2: LP+CPO**	**Case 3: HP+CPO**
Feedstock (TPD)	223	209	202
Power Capacity(MWe)	9.732	9.732	9.732
Power Produced (MWh)	72,464	72,464	72,464
Thermal Capacity (MWth)	9.596	9.596	9.596
Thermal Produced (MWh)	71,452	71,452	71,452
CAPEX			
Feeding System ($k)	$ 237.8	$ 237.8	$ 2,172.3
Gasifier ($k)	$ 10,624.0	$ 10,624.0	$ 5,312.0
Cleanup system ($k)	$ 8,499.2	$ 6,799.4	$ 5,099.5
Engine ($k)	$ 7,920.0	$ 7,920.0	$ 7,920.0
Other ($k)	$ 8,000.0	$ 800.0	$ 800.0
Total	$35,281	$26,381	$21,304
OPEX			
Feedstock ($/MWh)	$ 45.0	$ 42.2	$ 40.7
O&M ($/MWh)	$ 8.6	$ 8.6	$ 8.6
Labor ($/MWh)	$ 15.8	$ 14.9	$ 14.3
20yr L-CAPEX ($/MWh)	$ 24.3	$ 18.2	$ 14.7
Cost of Electricity ($/MWh)	$93.7	$83.9	$78.2

Based on this analysis, the following observations can be made:

- The use of CPO tar cracker provides a cheap and efficient solution to biomass gasification tar clean up problem.
- The use of GE's Posimetric® pump can further reduce the biomass gasification system capital costs.
- As a result, the CAPEX for case 1 at 9.7MWe scale is expected to be about $35MM, $26MM for case 2 and $21MM for case 3.
- The cost of electricity for case 1 is estimated at $93.7/MWh, $84/MWh for case 2 and $78.2 for case 3.

The above analysis demonstrated a clear economic entitlement of using a catalytic partial oxidizer for tar removal in biomass power generation system.

1.2.3 Sensitivity Analysis on Scale

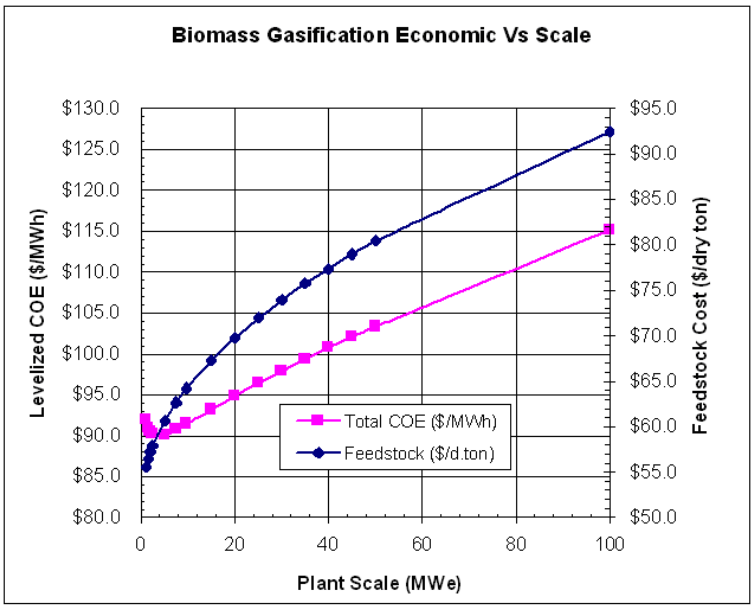

Figure 5 Biomass gasification economics at different scales

During this year, a sensitivity analysis was performed to study the effect of scale on biomass gasification system economics. Typically, economic of scale can be achieved by increasing the power plant capacity of a distributed biomass gasification system. However, due to the low energy content in biomass and the high transportation costs, the feedstock cost quickly becomes a dominating factor in system economics as the plant scale increases.

In this study, we used a typical "returns to scale" for a distributed power generation system and performed a simple "crop circle" analysis to evaluate the net economics impact resulted from these two contradicting factors.

As shown in Figure 5 and in Table 4, as the plant capacity increases from 1MW to 100MW, although the unit capital cost continue to decrease, the feedstock cost increased from $55.5/dry ton to about $92.4/dry ton. This dramatic increase in biomass feedstock cost is primarily due to the increase in transportation costs from longer distance. It is estimated that the average hauling distance increase from 5.1miles for 1MW plant to about 50.8 miles for 100MW plant. In another word, the economics of scale in distributed biomass gasification system is quickly offset by the increase in biomass feedstock cost, resulting in generally a higher cost of electricity at 100MW scale than at 10MW scale. Therefore, a small-scale (1~20MW) distributed biomass gasification power plant is likely to be more economical than a larger scales (100MW), primarily due to availability and cost of biomass feedstocks.

Table 4 Cost of electricity breakdown for different scales

Power Output (MW)	**1**	**5**	***10***	**20**	**30**	**50**	***100***
Levelized CAPEX ($/MWh)	$ 33.5	$ 26.3	*$ 23.8*	$ 21.4	$ 20.1	$ 18.6	*$ 17.8*
Operation ($/MWh)	$ 19.1	$ 20.9	*$ 22.1*	$ 24.1	$ 25.5	$ 27.7	*$ 31.9*
Feedstock ($/MWh)	$ 39.3	$ 42.9	*$ 45.5*	$ 49.4	$ 52.3	$ 57.0	*$ 65.5*
Feedstock ($/d.ton)	*$ 55.5*	*$ 60.6*	*$ 64.2*	*$ 69.8*	*$ 73.9*	*$ 80.4*	*$ 92.4*
Total COE ($/MWh)	**$ 92.0**	**$ 90.1**	***$ 91.4***	**$ 94.8**	**$ 97.9**	**$ 103.3**	***$ 115.2***

2. Tar Conversion Experimental Set-up

2.1 Experimental Work at GE

2.1.1 Test Rig Design and Fabrication

A lab-scale CPO test rig was designed to experimentally validate the conversion rate and efficiency of surrogate tar compounds from biomass gasifier. A system model written for ASPEN analysis was prepared based on air blown fluidized bed gasifier and the model provided surrogate tar content in biomass product stream and its major components. The ASPEN model also served to provide the basis for identification and sizing of individual components of CPO test rig.

Table 5 Syngas composition derived from an air blown biomass (wood pellets) gasifier

Component	Mol%
H_2O	7
N_2	36
H_2	23
CO	25
CO_2	9

A process and instrumentation diagram (P&ID) was prepared to provide detailed engineering information needed to construct the test rig and is shown in Figure 6. The test rig consists of 1) feed control, mixing and preheating, 2) CPO reactor, and 3) product stream quenching and analysis. Baseline CPO test condition with the gas hourly space velocity of 200,000/hr was used to size the mass flow controllers, CPO catalyst, reactor tube, chillers and volumetric flow meter in the test rig. Controlled flow of gases and liquid water enters an electrically heated vessel to preheat the steam-gas mixture before entering the CPO reactor tube. Also, the sizing of the mass flow controllers and steam generation was determined to cover a wide range of O/C and H_2O/C ratios in tar-air-steam mixture of CPO feed stream. The CPO feed introduction into a CPO reactor tube is schematically explained in Figure 7. A stream of liquid tar enters a “Nebulizer” and is subsequently atomized and mixed with air before reaching CPO catalyst within the CPO reactor tube. A mixture of preheated gaseous stream and steam also enters the reactor tube as shown in Figure 7 and is subsequently mixed with atomized tar-air. The position of the nebulizer tip inside the reactor tube was adjusted in order to achieve an ideal spray pattern and uniform mixing between components. As shown in Figure 7, a pair of Cajon Ultra Torr fitting was modified to accommodate Nebulizer and preheated gas stream introduction into the reactor tube and provide gas tight seal. The modified fitting also has two small ports for insertion of thermocouples, which measure the mixture preheating temperature and catalyst inlet temperature, respectively. A 25 mm OD quartz tubing served as the reactor tube. A CPO catalyst foam, 20 mm in diameter and 10 mm in length, was loaded inside the reactor tube and a blank ceramic foam was placed on top of the catalyst foam to promote CPO feed mixing and reduce radiation heat transfer from the catalyst foam. The location of CPO catalyst within the reactor tube relative to the furnace mounting was adjusted for optimized CPO feed mixing and preheating. A thermocouple located close to the bottom of the catalyst foam measured the CPO product stream temperature as it leaves the catalyst foam. Once the CPO feed mixture passed through the CPO catalyst foam, then the product stream was directed to condensers installed in series. While flowing through the chillers (can go as low as -15^{o}C to ensure complete condensation), the CPO product stream was cooled, and the

condensable part of the stream was collected by traps attached to individual condensers. Once the product stream left the condensers, it was directed to a volumetric flow measurement before being ventilated. Liquid condensate was analyzed using a DHA (direct hydrocarbon analyzer, Analytical Controls BV) and gas stream was injected to a Micro-Gas Chromatography (Agilent) and an RGA (residual gas analyzer, Analytical Controls BV) for compositional analysis. The collection rate of liquid condensate and gaseous flow rate measurement of CPO product stream coupled with compositional analysis provide information that was used for calculation of the conversion rate of tars and its conversion efficiency. Separate measurement of tar surrogate and liquid water vessel weight was performed over the duration of the test to double check the accuracy of feeding rate. The flow rate and compositional analysis was employed to validate the accuracy of the measurement by checking the material balance of element of interest (Carbon, in this task).

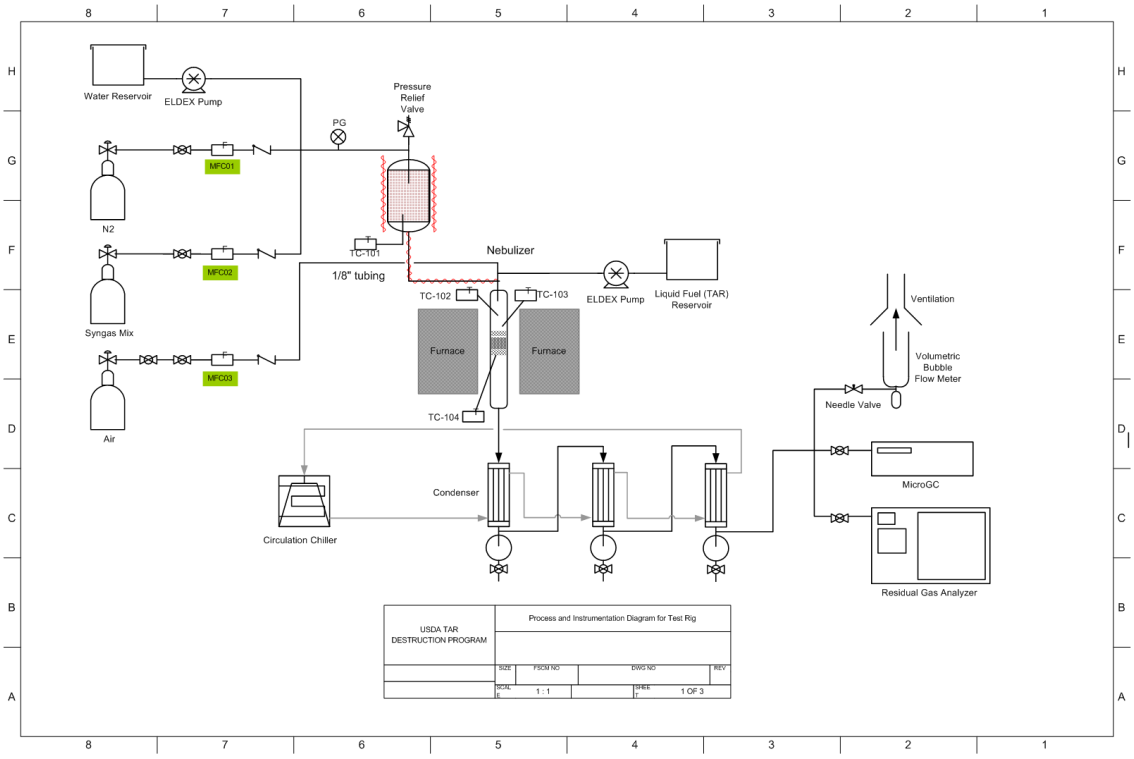

Figure 6 Process and instrumentation diagram for tar CPO conversion test rig

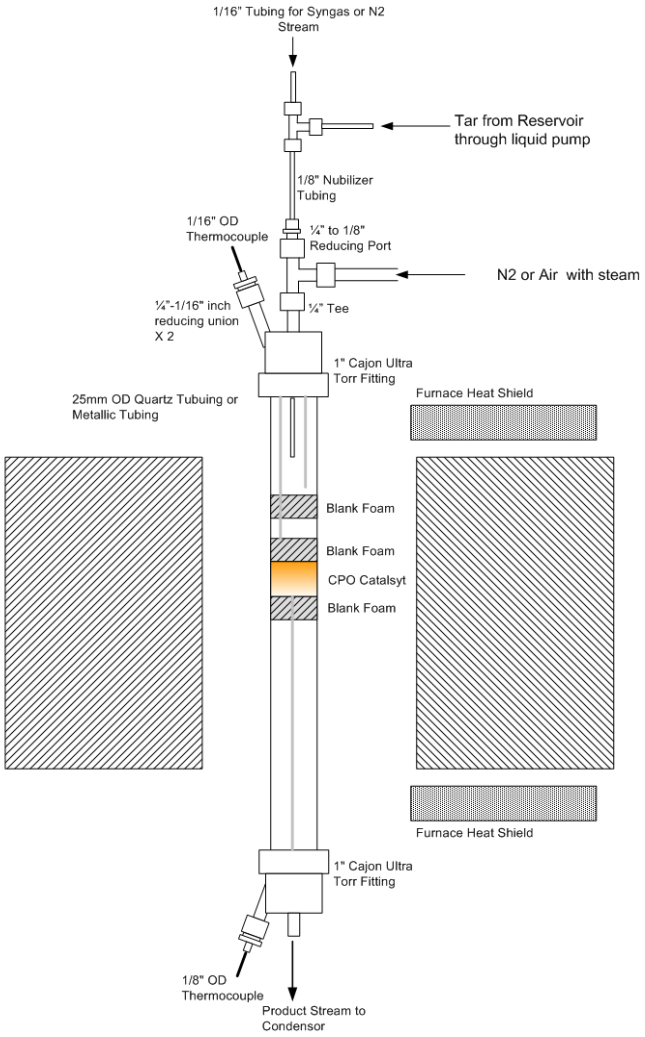

Figure 7 Test rig reactor assembly

The image of CPO reactor assembled and installed on the test stand is shown in Figure 8 (a). As shown in the figure, both the bottom and top section of the reactor was shielded by protective screen to avoid hot area contact and protect operator in case of quartz reactor rupture. Also shown in Figure 8 (b) are metering pumps for tar surrogate and Figure 8 (c) a condenser and trap assembly that chill the product stream for unconverted tar surrogate condensation and collection.

A Labview^{TM}-based data acquisition system was built and connected with thermocouples and pressure gauges to provide experimental data logging over the duration of test period. Especially, temperature readings inside the quartz reactor provided information that can be used to determine the operability of the reactor under given process conditions and the CPO catalyst performance.

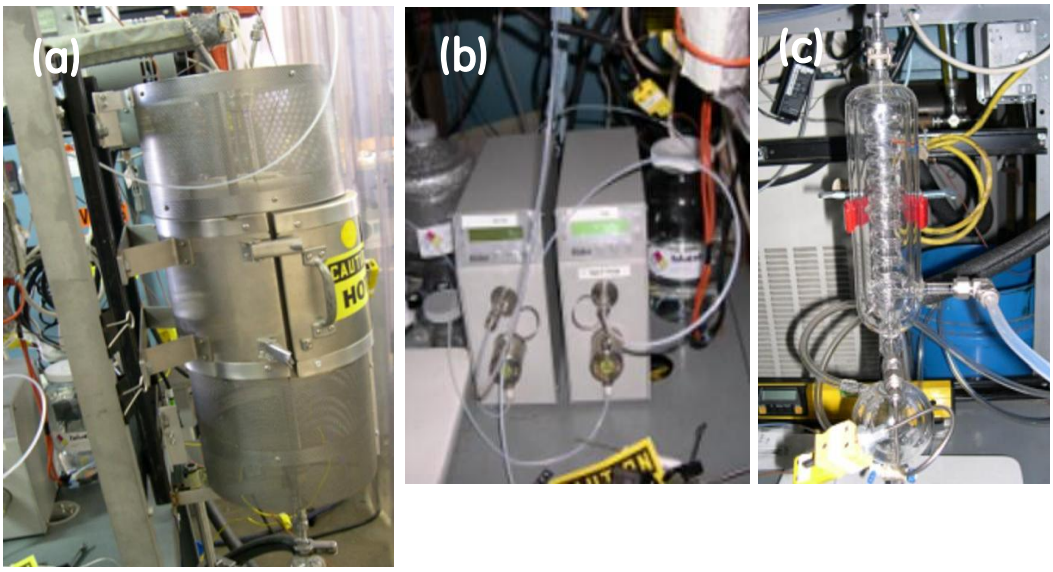

Figure 8 Images of major components of tar CPO conversion test rig

2.1.2. Test Rig Safety Review

In parallel with effort for design and fabrication of a lab-scale CPO tar conversion test rig, a comprehensive EHS (Environmental, Health and Safety) review of the Tar CPO test rig

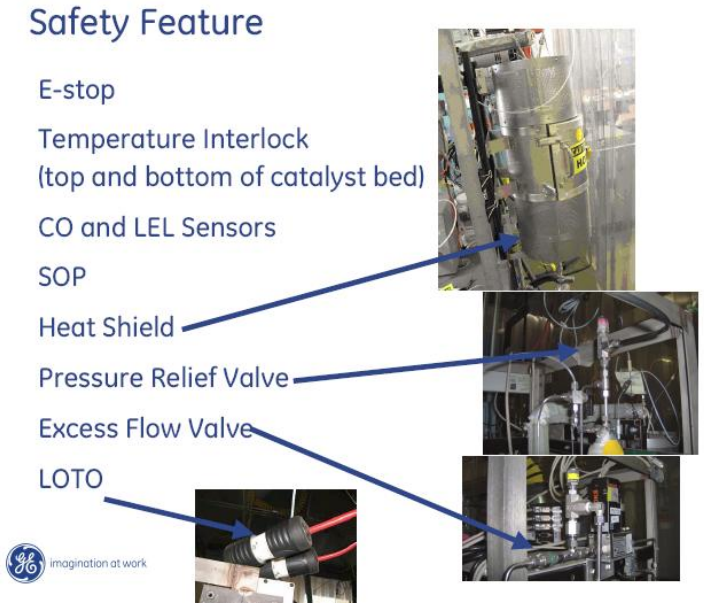

Figure 9 Safety features of the tar CPO test rig design and operation

was performed. The review was to ensure that the fabricated test stand follows GE's strict safety guidelines and its operation ensures safety through engineered design of test stand and operation procedure. The review included standard operation procedures (SOP), P-19

Chemicals (specifically, CO), White Tag review, Chemical Laboratory Audit Checklist and Facilities Project Safety Review Checklist. The review team included personnel involved in program execution and GE's internal EHS team.

SOP is a comprehensive manual that guides the operator for safe operation of the test rig. It includes piping and instrumentation diagram (P&ID), test area layout, details on functionality of major instruments, operation steps including start-up and shut-down, emergency response, system safety interlock and material safety data sheets (MSDS) of the chemicals being used. It also includes detailed operational procedure that requires operator's attention. Figure 9 shows the major safety features brought to the test rig design and operation.

2.1.3. Test Stand Component Shakedown

Upon the completion of safety review, all individual components in the test stand were evaluated to ensure its functionality during subsequent experimental tests. Below is a list of items that have been examined during system shakedown.

- Two metering pumps (Eldex) for water and tar delivery respectively: Based on calculated experimental conditions, relatively low liquid flow rates (<1 mL/min) will be used for the test. Therefore, both pumps were evaluated so that a reliable and accurate delivery can be achieved. The pump flow rates were calibrated according to the set points shown on the display panel.
- Mass flow controllers (MFC): Currently there are three MFCs installed. They are for delivery of three types of gases: Air, Nitrogen and Syngas mixtures. Each MFC was calibrated for their flow rates. The flow rates were within the flow ranges required by the experiments.
- Water bubbler and pressure relief valve: A pressure relief valve was installed before the upstream gases enter the water bubbler to eliminate potential damage to downstream component, particularly the quartz reactor. The pressure relief valve was set at 15 psi and tested for its functionality. This ensures that downstream pressure is maintained below 15 psi during the operation.
- Tar nebulizer: A nebulizer was used to atomize the tar liquid and spray the liquid uniformly before it reaches the catalyst bed. It has been tested for proper operation.
- High temperature furnace and temperature controller: The furnace can be ramped up to 1000^{o}C gradually regulated by the temperature controller.
- Circulating chiller: A circulating chiller that can be operated sub-ambient is used to condense the steam eluting out from the reactor. Unconverted tar, steam and other potential condensable liquid products can be removed so that they will not enter the gas analyzer downstream and cause any damage. The liquid portion can be analyzed through a direct hydrocarbon analyzer (DHA).
- Cooling water pump: An ice water pump is used to provide additional quenching of the stream.
- Gas chromatograph (GC): This is used to analyze the gas species present in the stream out of the reactor. The GC has been calibrated for different gas compounds possibly present in this reaction system, including CO, CO_2, H_2, N_2, O_2, C_2H_4, C_2H_2 and C_2H_6.

2.1.4. Catalyst Preparation

α-alumina foam supports of 99.5% purity purchased from Vesuvius High-Tech Ceramics were used for CPO catalyst. The support had a porous structure of 80 pores per inch (PPI) and its dimension was 20 mm in diameter and 20 mm in length. Washcoat was applied onto the substrate for increased surface area and catalyst dispersion. Prior to washcoat, the foam support was soaked in diluted HNO_3 solution, rinsed with deionized water, and dried in a cleaning step. The washcoat slurry consisted of high surface area alumina powder from Alpha Aesar and other metal oxide powders as dopant in small quantities. After dipping the foam in washcoat slurry, the foam was dried in a vacuum oven at 80^{o}C. Dipping and drying of the foam

was repeated until targeted washcoat loading was reached. The washcoated foam was calcined in air at 600°C and washcoat loading of 3% by weight was attained. The internal void fraction of the foam was experimentally determined. A diluted mixture of precursor solution of $Rh(NO_3)_3$ (Alfa Aesar) and $Ce(NO_3)_3$-$6H_2O$ (Alfa Aesar) was prepared for incipient wetness impregnation of the foam to attain 1 wt% Rh – 2 wt% Ce catalyst locating by weight. Half of the solution was impregnated on one face of the catalyst, followed by drying at 80oC in a vacuum furnace. The other half of the solution was impregnated from the other face of the foam and subsequently dried in the same manner. The catalyst was calcined at 600°C for 6 hours before testing.

2.2. Experimental Work at University of Minnesota (UoMn)

2.2.1. Test Stand Set-Up

Efforts thus far focused on the preparation of a reaction system for the short contact time reforming of a model gasifier effluent stream at representative temperatures (600-1000°C). Benzene has been selected as the model tar compound because of its high concentration in most gasifier effluents, generally comprising ~1/2 wt% of all undesired byproducts.

In order to accurately model a gasifier product stream, the system must be equipped with:

- Two liquid pumps for the delivery of H_2O and C_6H_6 (immiscible) to the system.
- Four mass flow controllers for the delivery of N_2, CO, CO_2, and H_2 to the system.
- Heated quartz (inert, temperature resistant) tubes to vaporize H_2O and C_6H_6 when fed to the system.
- Two nebulizers, capable of generating a fine uniform fine mist of H_2O and C_6H_6, eliminating pulsing and facilitating vaporization when fed to the system.
- The model gasifier effluent must then be heated to representative gasifier effluent temperatures (~600-1000°C), before entering the catalyst bed for reaction, requiring:
- A quartz reactor tube containing the noble metal based catalyst.
- Two thermocouples, placed at the front and back faces of the catalyst bed to measure feed gas and product gas temperatures.
- One tubular laboratory furnace capable of achieving high temperatures and high heating rates. This furnace will be connected to a PID controlled power supply that will hold the front face catalyst temperature constant by monitoring the thermocouple.

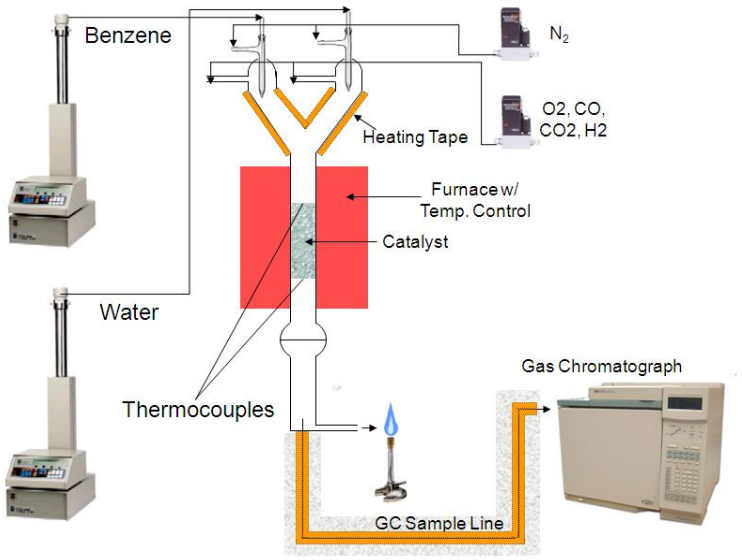

Figure 10 Reaction system for the study of tar reforming using traditional gasifier effluents

The reaction apparatus is represented graphically in Figure 10. The feed liquids and gases are fed to a heated quartz Y-splitter (wall temperature held constant at 325°C) where the liquids are vaporized and all gases are mixed before proceeding to the primary reactor tube. The gases are then rapidly heated to a desired temperature between 600 and 1000°C with accuracy of ±1°C before entering the catalyst bed. The catalyst bed length for preliminary experiments was 5 cm, in an 18 mm ID reactor tube. The tube size was later changed in order to accommodate different sizes of catalyst samples. The reactor effluent is pumped through a heated sample line directly to an HP 6890 gas chromatograph, calibrated to quantify H_2, O_2, CO, CH_4, CO_2, and C_6H_6 (using N_2 as the internal standard).

2.2.2. Catalyst Preparation

CPO catalyst employed for the test was 0.5 wt% Rh and 0.5 wt% Rh with 1 wt% Ce supported on 65 ppi α–Al_2O_3 foram. The foam was 17 mm in diameter and 10 mm in length. Rh and Ce were dissolved in distilled water as $Rh(NO_3)_3$ and $Ce(NO_3)_3{\cdot}6H_2O$ respectively, before being impregnated to the α-Al_2O_3 foam in a drop wise manner. Once dry, the catalyst was calcined for 6 hours at 600^{o}C. Catalysts were conditioned for approximately 1 hour under targeted test condition before acquisition of performance data.

3. Catalytic Tar Conversion Performance Evaluation Results and Discussion

3.1 Results Accomplished in Task B

Planned Activities: Biomass gasification tests, product characterization, and CPO tar conversion catalyst preparation. This task was conducted after completing process design and system economics analysis (Q3 2009 ~ Q4 2009). Major milestones include identification of syngas cleaning requirements for proposed system design, identification and selection of tar compounds and mixtures for use in CPO tests, and preparation of CPO catalysts for validation. This task has been completed at the end of Q4. CPO catalyst preparation has been described in detail in the Experimental section of this report.

Based on literature search and process design and analysis, the following feed compositions will be used for catalyst evaluation. As reported in Table 2, benzene and toluene are the two major compounds present in tar (37.9 wt% and 14.3 wt% respectively). Considering the toxicity of benzene and strict handling requirements (Classification: Health: 2, Fire: 3) in industrial laboratories, toluene has been used as the surrogate compound for the preliminary tests shown below:

- Toluene + Air + Steam (oxidation and steam reforming: does not require high preheat temperatures to achieve considerable conversions)
- Toluene + Steam (steam reforming: may require high preheat temperatures (>700^{o}C) to convert aromatics)
- Dry syngas + Toluene + Air + Steam (require extensive safety review to ensure safety operation)
- Dry syngas + Toluene + Steam

5-wt% toluene will be used for initial performance evaluation. Steam/Carbon ratio of 1 will be used as the starting point. O_2/Carbon ratio will be maintained below 0.5. The dry syngas composition is listed in Table 6.

Table 6 Simulated syngas composition used for experimental tests

Component	Mol%
CO	30
CO_2	5
H_2	20
N_2	45

3.2 Results Accomplished in Task C - GE

Planned Activities: Test CPO with biomass gasification product gas. Optimize CPO performance with selected tar compounds. Optimize CPO performance with multi-component mixtures. Milestones include optimizing CPO catalysts design, collecting CPO experimental data for next stage kinetic modeling and understanding the effect of relative reactivity on ultimate tar conversion and syngas yields. (Q1 2010 ~ Q3 2010)

Reaction system design and construction were described in the experimental section of the report. Tar conversion performance was evaluated through catalytic performance during tar steam reforming and partial oxidation reactions.

3.2.1 Steam reforming

Toluene steam reforming performance was evaluated on Rh-Ce-αAl_2O_3 catalysts. Toluene and water feed flow rates were metered by Eldex liquid delivery pumps. Toluene liquid was sent to a nebulizer. In the presence of high pressure created by the feed gas (nitrogen or syngas in

our studies), toluene can be atomized into uniformly distributed liquid drops and subsequently mixed with other reactants upon leaving the tip of the nebulizer. The water feed was directed to a steam generator, which is heated above 120°C. A carrier gas was used for the steam generator to ensure stable steam delivery to the reactor. This carrier gas could be either nitrogen (during steam reforming) or air (during catalytic partial oxidation).

Toluene flow rate was fixed at ~0.2 g/min, with ~5 wt% or ~1 mol% in the total feed stream. Steam/Carbon ratios were controlled by varying the water flow rate. For steam reforming experiments, in addition to toluene and water, nitrogen was used to atomize toluene and carry steam. Representative results were presented in Figure 11 and Figure 12.

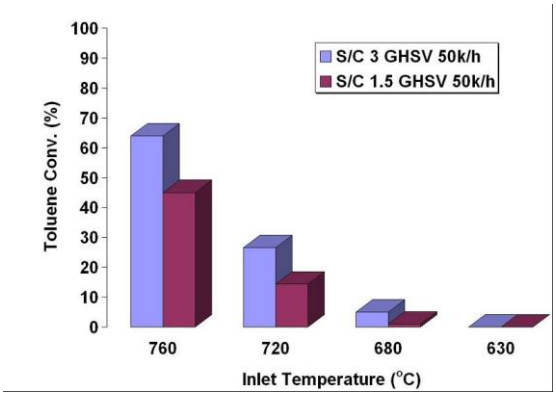

Figure 11 Effect of Steam/Carbon ratio on toluene steam reforming performance

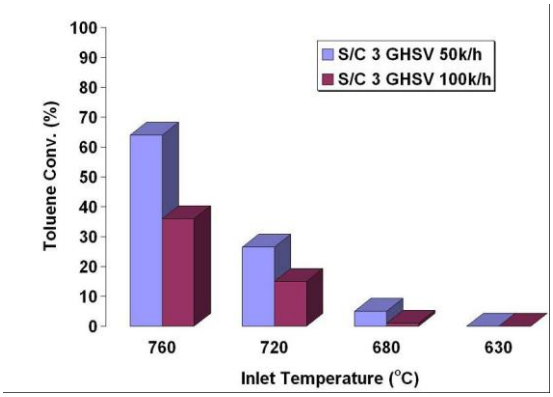

Figure 12 Effect of Gas Hourly Space Velocity (GHSV) on toluene steam reforming performance

As shown in Figure 11, steam-reforming performance was evaluated at different temperatures. The inlet temperature was measured by the thermocouple installed at the top of the catalyst bed. The Gas Hourly Space Velocity (GHSV) were maintained ~50,000 /hr for all experiments. The results showed that as the reaction temperature increased, more toluene can be converted during the steam reforming reaction, reaching ~65% toluene conversion at ~760°C when S/C is ~3. Lowering the S/C ratios diminished the steam reforming performance at the same temperature. Figure 12 studied the GHSV effects by employing GHSV of 50,000 /hr and 100,000 /hr during the test. Increasing in GHSV decreased the steam reforming catalytic performance. It should be noted that typical gasifier operates at a residence time of seconds scale. In our experiments, milliseconds residence time was used. Therefore, the small catalyst bed volume will be very small in comparison with the gasifier volume. This translates to reduction in catalyst cost in potential applications.

3.2.2 Catalytic partial oxidation

The steam reforming performance achieved in Figure 11 and Figure 12 are very promising considering the large GHSV we used. However, typical gasifiers operate between 700~800°C and the gasifier outlet temperatures would be below 700°C. A further improvement is needed for the catalysts capable of operating at lower temperatures while maintaining similar conversions. To accomplish this goal, a certain amount of air was injected in addition to steam. As shown in Figure 13, with air injection, even at catalyst temperatures as low as 420°C, a 45% toluene conversion is obtained. The presence of air is beneficial for the reaction at low temperatures. Air enhances the catalyst surface temperature by reacting with toluene and releasing heat locally through combustion.

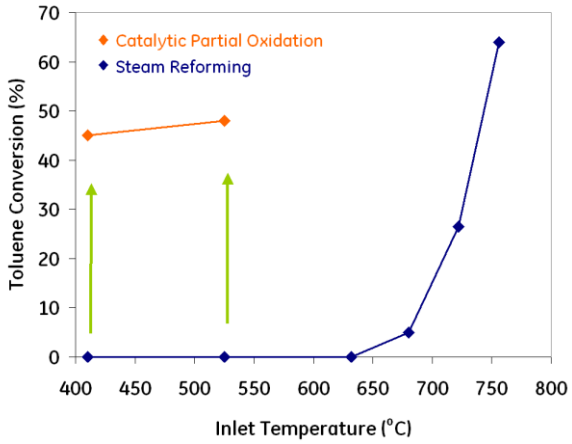

Figure 13 Comparison of Catalytic Partial Oxidation and Steam Reforming in their tar conversion performance (GHSV ~ 55,000 /hr, S/C=3, CPO air addition: O/C ~2)

In 2010, catalytic tar removal reaction operating parameters were optimized using selected tar compounds. An understanding of how inorganic impurities present in biomass gasification raw syngas was acquired under this program as well. Below is a list of parameters studied under Task C. Those experiments were designed in order to understand the complex reaction network with the tar removal system. Both 1-Methyl-Naphthalene (MN) and Toluene (T) (Their structures are shown in Figure 14) were used as tar compounds. Rh-Ce-Al_2O_3 foam catalyst was used for all experimental runs.

- Presence of air and O/C effect: Tar + Steam + Syngas, with or without air, varying furnace preheat temperature
- Presence of syngas: Tar + Air + Steam + with or without syngas
- Effect of steam: Tar + Air + Steam + Syngas, varying steam concentration
- Performance at different GHSVs: Tar + Air + Steam + Syngas, varying GHSV
- Effect of catalyst L/D ratio: Tar + Air + Steam + Syngas, varying L/D ratio
- Inorganic impurities

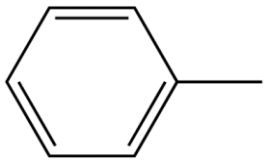

T: Toluene

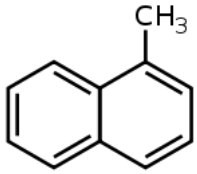

MN: 1-Methyl-Naphthalene

Figure 14 Structure of Toluene and Methyl-Naphthalene

3.2.3 Presence of air and O/C effect

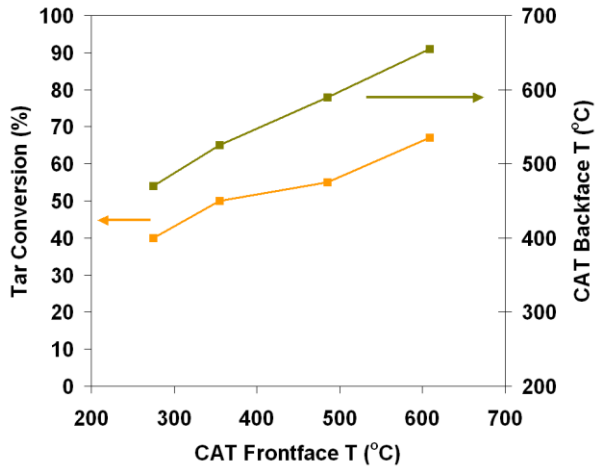

Figure 15 Toluene conversion & catalyst backface temperature profiles as a function of catalyst frontface temperatures (S/C ~3, O/C ~1.5)

Two sets of experiments were conducted. In one experiment, tar conversion data at different temperatures were collected with the presence of steam and syngas (i.e. steam reforming). Results showed no measurable tar conversion until catalyst frontface temperature reached 650°C. Another finding is the occurrence of the water-gas shift reaction at lower temperatures (<650°C), as evidenced from the relative ratio change between CO, H_2 and CO_2.

In another experiment, with tar (toluene), syngas and steam flow rates maintained the same as above, air was introduced to the reactor at an O/C ratio of 1.5.

As shown in Figure 15, a 40% toluene conversion was detected when the catalyst frontface temperature was 300°C. This was accompanied by a ~470°C backface temperature. The toluene conversion further increased as temperature was raised. It can be seen that presence of air is important for activation of toluene. Tar can be converted relatively easily at lower temperatures with air in the feed. On the other hand, steam reforming of simulated tar and syngas gasifier mixtures has slow kinetics at low temperatures.

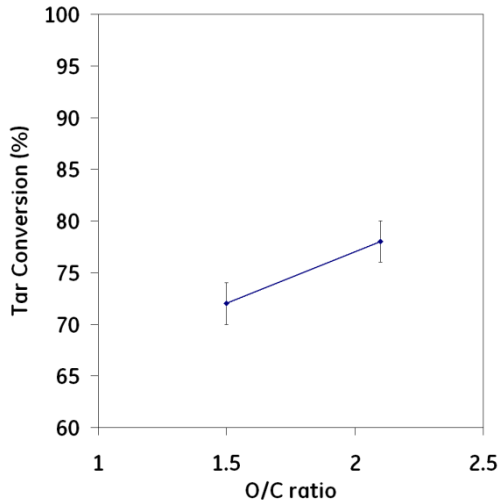

Figure 16 O/C effect on toluene conversion: GHSV=~35,000/h, S/C=3~3.5

Experiments were also run at different O/C ratios. As shown in Figure 16, when O/C increased from 1.5 to 2, an increase in tar conversion was observed. It was attempted to achieve further higher conversion by running the reaction at an even higher O/C. However, catalyst frontface temperature rapidly increased to above 850°C, which led to coking in the injector tip.

3.2.4 Presence of syngas

Experiments were run with syngas in the feed replaced with an equal flow rate of nitrogen. It was found that the tar conversion slightly dropped when syngas was removed from the feed. A change in the product distribution was also seen, with an increase in CO and decrease in CO_2 and H_2. The variation in product distribution can be attributed to product redistribution with the new feed mixture composition.

For the tar conversion reaction with both syngas and tar in the feed, it was speculated that as the feed is contacted with air and steam, O_2 may preferentially react with H_2 in the syngas instead of with tar, which was in much lower concentration and more difficult to crack. The initial reaction between syngas and air releases heat and rapidly raises catalyst surface temperature. The high temperature facilitated the conversion of tar with air and steam as it moved along the catalyst bed. Steam reforming of tar generated H_2 and CO. Water-gas shift reaction also kicks in to produce additional H_2 and CO_2

Because of the tendency for syngas to react with air, a concern would be a complete combustion of syngas in the feed. Efforts were made to examine the syngas concentration before and after the tar catalytic conversion system. As shown in Figure 17 and Figure 18, 60~70 g/Nm^3 tar compounds were introduced into the reactor system together with syngas, air and steam. An ~80% tar conversion was achieved for both reactions. For the gas composition, although initially a portion of the H_2 may be combusted, the overall H_2 concentration in both cases increased as a result of the tar reforming and water-gas shift. There was a slight decrease in CO concentration as a result of the water-gas shift reaction.

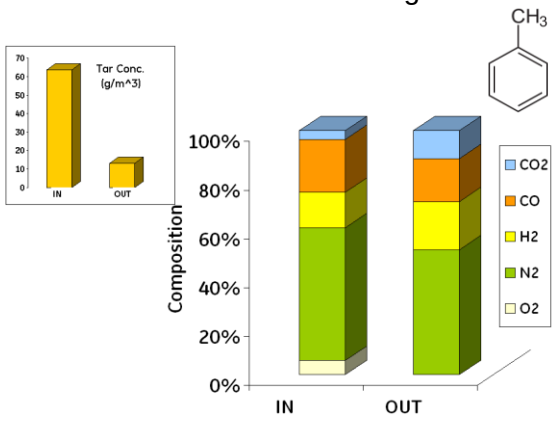

Figure 17 Inlet and outlet tar and gas compositions for toluene conversion reaction (GHSV = 75,000 /h; 20mm (D) by 10mm (L) Rh-Ce-Al_2O_3 foam catalyst; S/C = ~3; O/C = ~1.5)

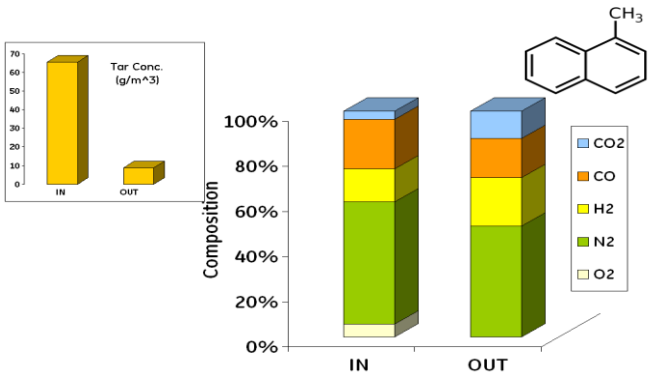

Figure 18 Inlet and outlet tar and gas compositions for methylnaphthalene conversion reaction (GHSV = 38,000 /h; 20mm (D) by 10mm (L) Rh-Ce-Al_2O_3 foam catalyst; S/C = ~3; O/C = ~1.5)

3.2.5 Effect of steam

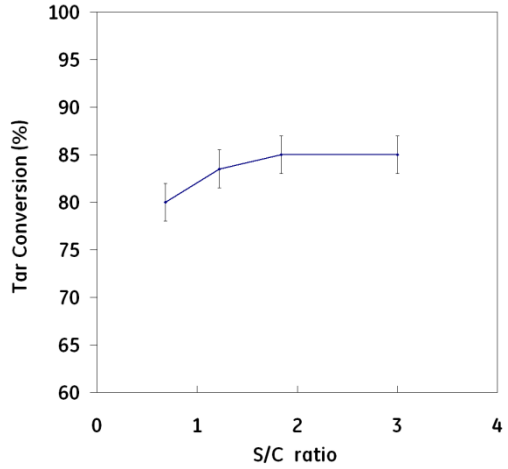

Figure 19 Methylnaphthalene conversion as a function of S/C ratio (GHSV = 35,000 /h; 20mm (D) by 20mm (L) Rh-Ce-Al_2O_3 foam catalyst; O/C = ~1.5)

The amount of steam in the feed was varied to evaluate its influence on the tar conversion. As indicated from Figure 19, tar conversion increased slightly when more steam is present in the feed. The influence of steam on product distribution is more pronounced. With more steam, there was a clear increase in H_2 and CO_2 production and a decrease in CO, implying that the water-gas shift reaction is favored with more steam.

3.2.6 Performance at different GHSVs

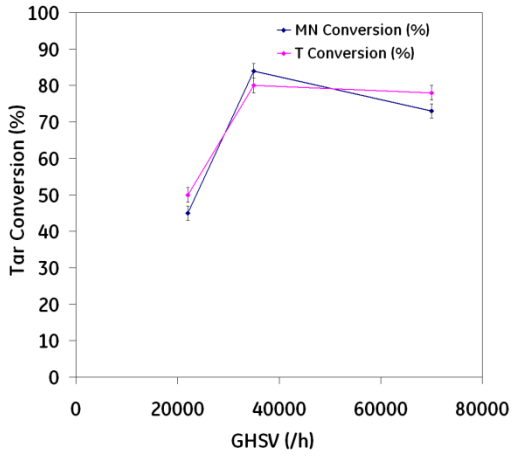

Figure 20 Comparison of tar conversion at different GHSVs for both compounds T and MN: S/C=~3, O/C=~1.5, 20mm (D) by 20mm (L) Rh-Ce-Al_2O_3 foam catalyst

As shown in Figure 20, for 20mm (D) by 20mm (L) foam catalyst, both tar compounds can be converted in similar conversion rates under the same operation conditions. Three GHSVs (residence time) were used: 22,000 h^{-1} (164ms), 35,000 h^{-1}(103ms), and 70,000h^{-1}(51ms). As GHSV increased, the tar conversion (for both MN and T) first increased and then started to decline as space velocities further increased. Catalyst front and backface temperatures were also plotted as a function of GHSV (Figure 21 and Figure 22). At lower GHSV, the catalyst demonstrated a uniform temperature, with front and backface temperatures equal or very similar. A steep temperature gradient was observed at higher GHSVs.

This observation is similar to the finding reported by Schmidt et al.[3]. In their studies, at space velocities near 10^5 h^{-1}, the front and back temperatures were roughly equal. When space velocities increased to above 4×10^5 h^{-1}, a steep temperature gradient was measured. This behavior is known as blowout. In the event of a blowout, heat is removed from the surface faster than what is generated by the reaction. This results in a large temperature gradient between the top and bottom of the catalyst, accompanied by low methane conversions and syngas selectivities. The conclusions presented in Schmidt et al.'s paper supported our experimental findings as shown in Figure 21 and Figure 22.

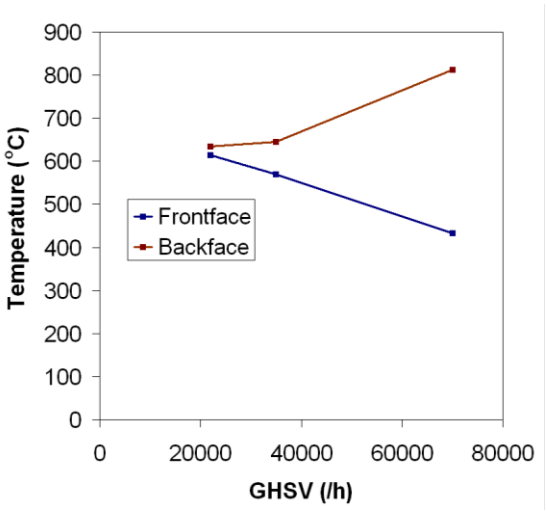

Figure 21 Catalyst frontface and backface temperatures as a function of GHSV for methylnaphthalene conversion experiments

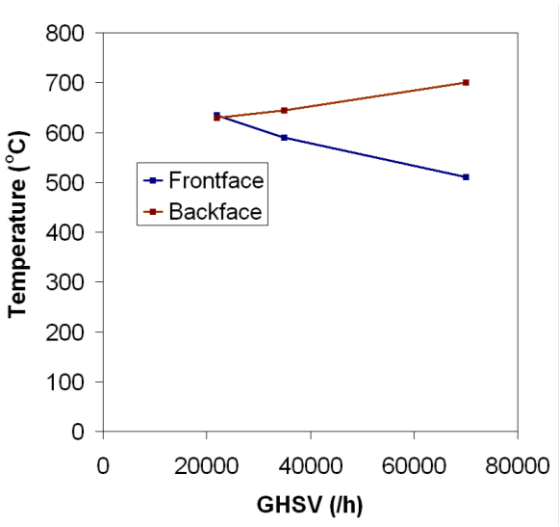

Figure 22 Catalyst frontface and backface temperatures as a function of GHSV for toluene conversion experiments

3.2.7 Effect of catalyst L/D ratio

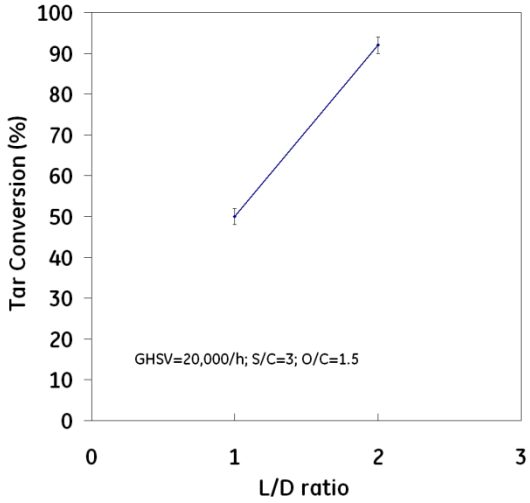

Figure 23 Toluene conversion as a function of L/D ratio: ~115 g tar/m^3syngas, Rh-Ce-Al_2O_3 foam catalyst, S/C=3, O/C=1.5, GHSV=20,000/h

Catalyst Length/Diameter (L/D) ratios largely impact the tar conversion: At L/D=2, an over 90% tar conversion can be achieved, which makes our tar removal technology highly promising for clean syngas production. As shown in Figure 23, under the same operating conditions, when L/D was changed from 1 to 2, a dramatic increase in tar conversion was measured (50% vs. >90%).

Figure 24 and Figure 25 are the time on stream plots using L/D=2 Rh-Ce-Al_2O_3 foam catalysts. Both toluene (T) and a mixture of T and methylnaphthalene (MN) were evaluated. Carbon conversion is defined as the conversion of carbon in tar compounds. In Figure 24, a 90-95% tar conversion was achieved.

In Figure 25, a T and MN mixture was used as tar compounds. As shown in the figure, catalytic performance was steady at ~60% carbon conversion. Therefore, it can be concluded that keeping a higher L/D ratio helps the tar conversion. It allows sufficient time for the reactants to contact and react along the catalyst bed.

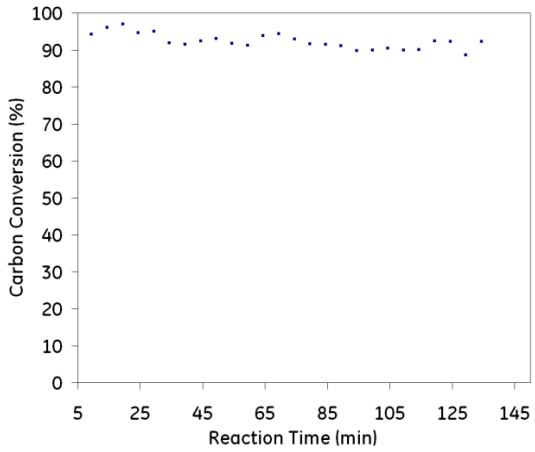

Figure 24 Toluene conversion as a function of time on stream: toluene in syngas (115 g tar/m^3syngas); 20mm (D) by 40mm (L) Rh-Ce-Al_2O_3 foam catalyst; O/C = ~1.5; S/C = 3~4, GHSV ~20,000/h

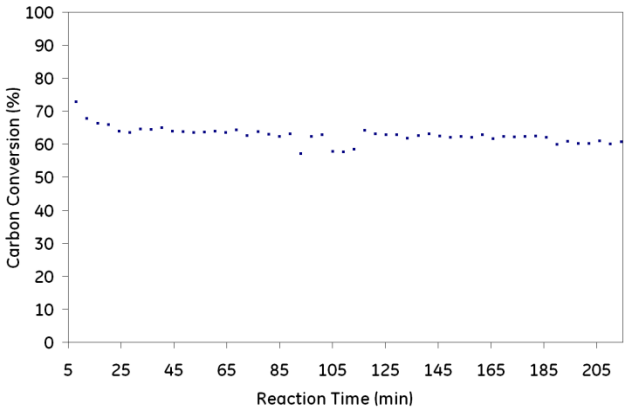

Figure 25 Carbon conversion as a function of time on stream: Mixture (1:1 by weight) of Toluene and Methyl-naphthalene with a total of 136 g tar/m^3syngas; 20mm (D) by 40mm (L) Rh-Ce-Al_2O_3 foam catalyst; O/C = ~1.5; S/C = 3~4

3.2.8 Inorganic impurities

One important objective of this program is to evaluate the effect of impurities' on tar conversion performance. Our collaborator, the University of Minnesota, has conducted extensive studies using a series of impurity elements. This section summarizes understandings that GE and UoMn have developed on how impurities present in biomass gasification influence the reforming catalyst.

As shown in Figure 26, biomass contains a variety of inorganic elements. During the gasification process, these elements enter either the gas or the solid phases. From literature studies and understandings acquired through other research projects in our laboratory, the main inorganic impurities present in solid ash are K, Na, Mg, Ca, P, S, Cl and Si. Syngas, tar, particulates, and inorganic elements including Na, K, Cl and S, exit the gasifier in the gas phase. After the biomass gasifier, typically there is a ceramic filter and alkali adsorbent bed to remove a major portion of the tar, particulates and inorganic impurities. As reported by Corella et al.[4], a ceramic filter (operating at 500-600^{o}C) followed by a calcined dolomite bed, effectively eliminates 90-95 wt% of the tars present in flue gas. Therefore, tar concentration can be reduced to approximately 0.5-1.0 g/nm^3. The alkali sorbent can reduce Na and K concentration to less than 1 ppm[5]. The syngas stream coming out of the filter and sorbent bed is then routed to a tar converter. The tar converter is used to eliminate tars by converting them into additional syngas. How impurities affect the performance of the catalytic tar converter is an important topic in this gas clean-up strategy.

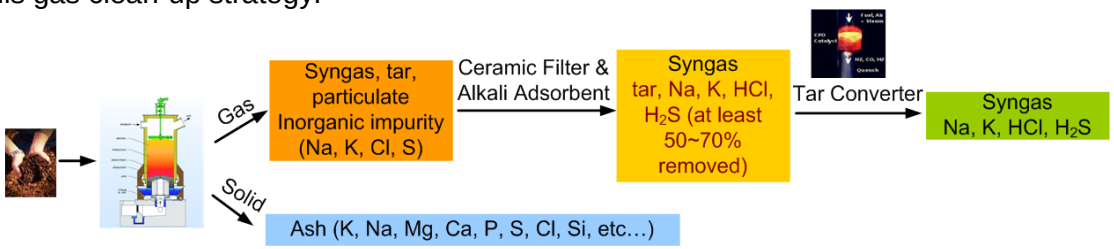

Figure 26 Gas clean-up for biomass gasification

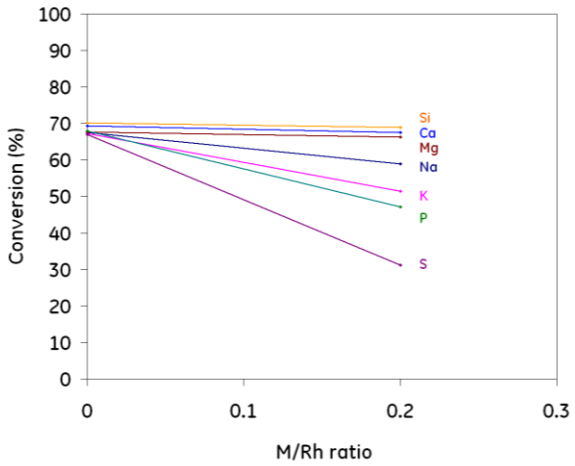

Figure 27 Influence of inorganic impurities on carbon conversion as a function of M/Rh ratio (M is the inorganic element)

University of Minnesota used steam methane reforming to screen the effects of impurities on the catalyst performance. Inorganic impurities were impregnated onto the surface of Rh-Al_2O_3 catalyst in a defined ratio. Figure 27 shows CH_4 conversion as a function of M/Rh ratio for different inorganic impurities. Below are findings from the tests.

- Si, Ca, Mg: Minimal impact on catalyst performance
- Na, K: Moderate effect when a high amount was directly impregnated on catalyst surface; In typical syngas mixtures, Na, K is less than 10 ppm and can pass through the catalyst due to high temperature.
- P: Mostly stays in the ash
- S: When doped directly onto the surface, the sulfur significantly reduced the catalyst performance. In previous work it was shown the sulfur deposition is dependent on surface temperatures.

Due to the potential instrument damage from gas phase impurities depositing onto instrument surfaces, impurities were impregnated onto the catalyst surface instead of mixing with the gas phase. It should be noted that a high impurity concentration was used during the experiments in order to get measurable effects. Therefore, the impurity effects observed in Figure 27 can be viewed as an extreme situation when impurities in the gas phase are accumulated to a comparable amount as the Rh active metal on the surface. The actual impurity inhibition effect may be less severe. From our previous experience, HCl and H_2S, at high temperatures such as those experienced in the reformers, pass through the catalyst directly instead of depositing onto the catalyst surface.

3.3 Results Accomplished in Task C - UoMn

It has been shown that similar CPO reactors have a distinct oxidation zone followed by a reforming zone in the catalyst.[6] The University of Minnesota team plans to investigate the activity of both reaction zones for tar conversion to synthesis gas. To investigate the performance of the reforming zone, a model gasifier product stream will be fed at representative temperatures to a noble metal based catalyst bed. Depending on the activity of the reforming zone, oxidation chemistry may be needed to achieve desired tar conversion to syngas. To investigate the performance of the oxidation zone, nitrogen and oxygen at air stoichiometry will be mixed with a model gasifier product stream and fed at representative temperatures to a noble metal based catalyst bed. It is desirable to minimize the amount of air co-feed required for complete tars conversion, as oxygen shifts the product equilibrium generating more complete combustion products. Experimental findings from this team were summarized below. It should be noted and acknowledged that some of the figures/discussions have been published in journal Energy & Fuels 2009, 24, 1341–1346(DOI:10.1021/ef901033d)[7].

3.3.1 Effect of Temperature and H_2O Concentration

The effect of temperature and water concentration in the feed on steam reforming activity was studied on Rh/α-Al_2O_3 and Ce-Rh/α-Al_2O_3 catalysts at five different temperatures. For all data presented, benzene feed concentration and total flow rate were held constant at 2-mol% and 2 SLPM respectively. For Rh catalyst (Figure 28 (A)), at 850 °C and 20-mol% H_2O in the feed, there is 50% C_6H_6 conversion. This value decreases with decreasing concentrations of water in the feed. Between 0 mol% and 10 mol% H_2O in the feed, C_6H_6 conversion has a strong dependence on H_2O concentration increasing linearly from 0% to 42%. Between 10-mol% and 20-mol% H_2O, C_6H_6 conversion has a weak dependence on H_2O concentration increasing from 42% to 50% over the entire range. The conversion of C_6H_6 decreases with decreasing front face catalyst temperature. There is zero observable catalyst activity below 15-mol% H_2O at 700°C, and for all H_2O concentrations at 650 °C. Additionally, at lower temperatures the increase in C_6H_6 conversion is relatively linear with increasing H_2O concentrations.

Ce was reported for its promotional function to stabilize, disperse, and transfer oxygen to the Rh catalyst sites[8, 9]. Rh-Ce catalyst was prepared and evaluated, with results shown in Figure 28(B). At 850°C and 15-mol% H_2O in the feed, there is nearly complete conversion of C_6H_6, a two-fold increase in activity compared to the Rh/α-Al_2O_3 catalyst. At this temperature, as the concentration of water in the feed is decreased, the conversion of C_6H_6 decreases, closely matching the maximum conversion expected according to the stoichiometry of benzene steam reforming reaction ($C_6H_6+6H_2O\rightarrow6CO+9H_2$).

At high temperatures on the Rh-Ce catalyst, water is limiting in the reforming reaction below 12-mol% H_2O in the feed. This contributes to an increase in C_6H_6 conversion dependence on H_2O concentration. Above 12-mol% H_2O, the stoichiometry of the feed does not prevent reforming from proceeding to completion, meaning surface reaction rates dictate the C_6H_6 conversion.

Similar to the Rh/α-Al_2O_3 catalyst, as the front face catalyst temperature decreases the activity of the catalyst decreases. However, the addition of Ce maintains catalytic activity at low temperatures and H_2O concentrations. This can be explained by the ability of Ce to increase rates of oxygen transfer by forming intermetallic compounds and storing oxygen, in addition to physically dispersing and supporting the Rh sites[10].

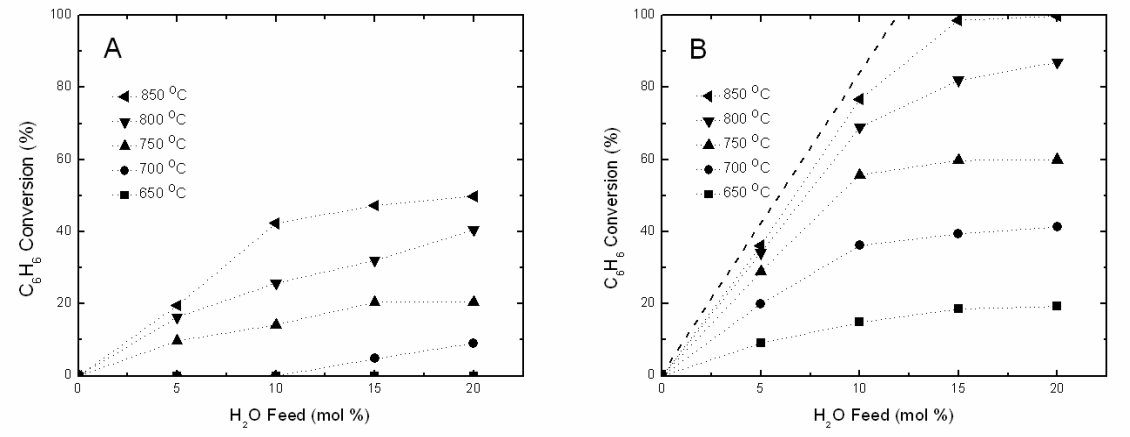

Figure 28 Benzene conversion as a function of H_2O concentration in the feed at five different catalyst front face temperatures. Panel A: Rh/α-Al_2O_3, Panel B: Rh-Ce/α-Al_2O_3[7]
Reaction conditions: 2 SLPM total flow, 2 mol% C_6H_6, variable H_2O concentrations, and the balance N_2.
The bold dashed line in Panel B represents the expected benzene conversion for 100% stoichiometric consumption of feed H_2O through steam reforming.

3.3.2 Effect of benzene concentration

The effect of C_6H_6 concentration in the feed on reforming activity was studied on an Rh-Ce/α-Al_2O_3 catalyst and presented in Figure 29. Temperature, steam concentration, and total flow rate were held constant at 750 °C, 10 mol%, and 2 SLPM respectively, while C_6H_6 concentration was varied between 1 and 4 mol% in increments of 1 mol%. At 1 mol% C_6H_6 in the feed there is 87% C_6H_6 conversion, corresponding to a C_6H_6 consumption rate of 7.2×10^{-4} mol min^{-1}. As the C_6H_6 concentration in the feed is increased to 4-mol%, the conversion drops to 20%. However, the total C_6H_6 consumption rate remains in a narrow range between 6.5×10^{-4} and 8.6×10^{-4} mol min^{-1}, exhibiting a weak dependence on C_6H_6 concentration under these conditions.

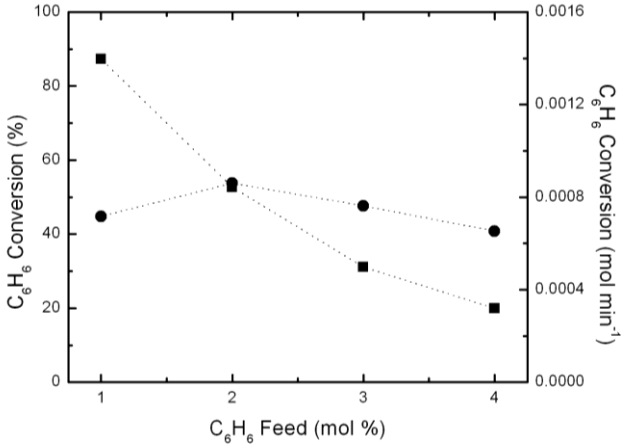

Figure 29 Benzene conversion rate and percent converted as a function of benzene concentration in the feed at 750 °C over a Rh-Ce/α-Al_2O_3 catalyst at 2 SLPM total flow, 10 mol% H_2O, variable C_6H_6 concentrations, and the balance N_2.

3.3.3 Effect of H_2, CO, and CO_2 co-feeds

The effect of H_2, CO and CO_2 co-feeds on C_6H_6 steam reforming activity was studied on an Rh-Ce/α-Al_2O_3 catalyst as shown in Figure 30. Temperature, steam concentration and total flow rate were held constant at 750 ºC, 10 mol%, and 2 SLPM respectively, while H_2, CO, and CO_2 concentrations were independently fed and varied from 0 to 20 mol% in the feed.

Co-feeding CO_2 to the system increased C_6H_6 reforming activity. At high CO_2 concentrations, C_6H_6 conversion was observed to increase by 7.6%. It is generally agreed that CO_2 has a strong positive influence on reforming activity. Co-feeding H_2 to the system had no observable effect on C_6H_6 reforming activity. From this it can be inferred that product inhibition through blocking of active sites by H_2 was negligible. Furthermore, due to small concentrations of CO_2 generated through C_6H_6 reforming, H_2 reaction with CO_2 through RWGS to generate additional H_2O for steam reforming was insignificant.

Co-feeding CO to the system decreased C_6H_6 reforming activity. At high CO concentrations C_6H_6 conversion was observed to decrease by 13%. There are two possible explanations for the observed decrease in activity. The first is that CO inhibits reaction by adsorption onto catalyst active sites[11]. The second is that dry reforming is a combination of RWGS and steam reforming[12] and the high concentrations of CO and H_2O in the feed drive the production of CO_2 and consumption of H_2O via WGS.

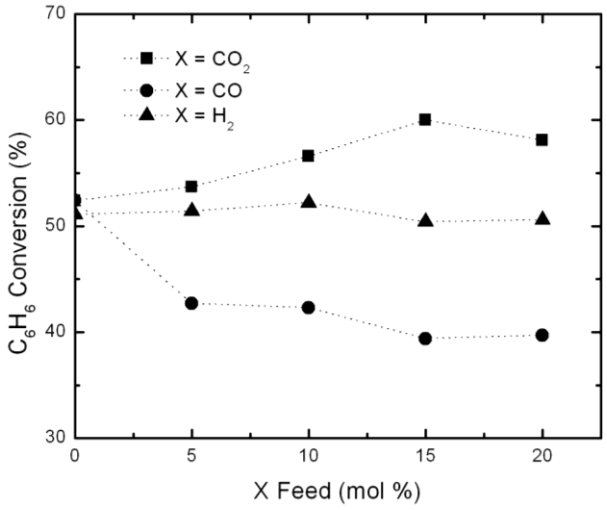

Figure 30 Benzene conversion as a function of CO, CO_2, and H_2 feed concentration at 750°C over a Rh-Ce/α-Al_2O_3 catalyst at 2 SLPM total flow, 10 mol% H_2O, variable CO, CO_2, or H_2 concentrations, and the balance N_2.

3.3.4 Simulated biomass-derived syngas

Experiments were performed using a representative biomass-derived syngas mixture over an Rh-Ce/α-Al_2O_3 catalyst at 2 SLPM total flow and 850°C. Feed and product information is presented in Table 7. Recommended feed concentrations[13] were reproduced as closely as possible within the limits of the experimental apparatus, using C_6H_6 as the model tar compound.

Results indicate nearly complete conversion of C_6H_6 in the reactor to a concentration of only 5 ppm. Products approached equilibrium at 2 SLPM total flow rate corresponding to a gas residence time of ~40 ms, which demonstrates minimal inhibition of reforming by the syngas co-feeds. In addition to nearly complete tar removal, the product stream contained 23.1 mol% H_2 and 27.8 mol% CO, an increase of 3.1 and 7.8 mol% respectively. The observed high conversions at low residence times may make the process appealing for scale up. However, long term experiments examining catalyst loss and deactivation are needed before considering such a process for commercialization.

Table 7 Experimental results for reforming of a typical biomass-derived syngas at 850°C on Rh-Ce/α-Al_2O_3 catalyst

Biomass Gasifier Product Stream				
Component	**Recommended by literature (mol %)**	**Reactor Feed (mol %)**	**Reactor Effluent (mol %)**	**Equilibrium Effluent (mol %)**
N_2	36.1	43.3	40.29	40.1
CO	24.6	20	26.3	27.8
H_2	22.4	20	23.55	23.1
CO_2	9.1	9.1	5.14	4.6
H_2O	6.6	6.6	4.69	4.3
Tars	~0.5-1	1	0.0005	0

3.3.5 XRD Crystal Phase Analysis

Experimental data were periodically repeated to test catalyst deactivation. After more than 40 hrs on stream, the Rh/α-Al_2O_3 catalyst exhibited no significant deactivation (C_6H_6 conversion remained within experimental error). XRD patterns are presented in Figure 31, Panel C for fresh and used Rh catalysts supported on α-Al_2O_3 monolithic foams. XRD patterns were also measured after crushing the catalysts into a powder to obtain a more averaged measurement over the entire catalyst (Figure 31, Panel A). Results were the same for both the monolith and powder measurements, and are presented normalized to the largest α-Al_2O_3 peak.

There is a clear increase in primary Rh peak height at 41.2° for the used catalyst (Figure 31, Panel A). The smaller peak for the fresh catalyst relative to the used one indicates that a higher fraction of the fresh Rh catalyst is in a more amorphous state, suggesting that the particles are smaller and more dispersed on the Al_2O_3 surface. The larger crystallites likely present in the used catalyst have low-index surface planes, reducing their activity relative to smaller clusters.

After more than 40 hrs on stream, the Rh-Ce/α-Al_2O_3 catalyst also exhibited no signs of deactivation. XRD patterns are presented in Figure 31, Panel C for fresh and used Rh-Ce catalysts supported on α-Al_2O_3 monolithic foams. XRD patterns for the ground Rh-Ce catalyst are also presented in Panel B of Figure 31. Results were the same in both the monolith and powder measurements, and are always presented normalized to the largest α-Al_2O_3 peak.

The lack of a significant Rh peak for the fresh and used catalyst indicates the Rh particles are highly amorphous, suggesting small particle sizes. Furthermore, there is essentially no difference in Rh peak heights between the used and new catalysts (Figure 31, Panel B), indicating that minimal catalyst sintering takes place during operation. The addition of Ce has been previously shown to physically stabilize and disperse Rh catalyst sites. These observations help to explain the increase in activity upon adding Ce to the catalyst.

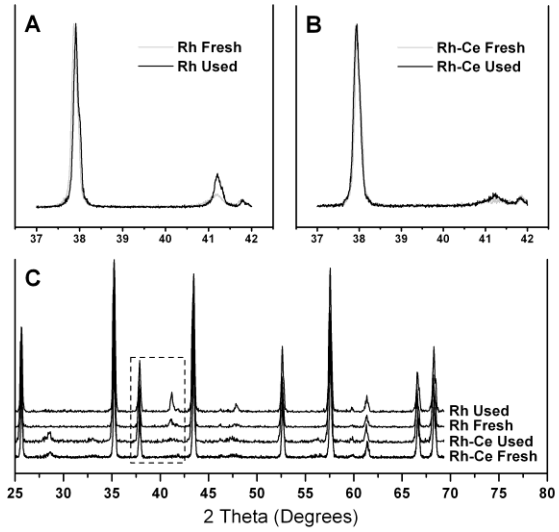

Figure 31 XRD patterns of Rh/α-Al_2O_3 and Rh-Ce/α-Al_2O_3 catalysts before and after use.
Note: All patterns are normalized to the largest peak (Al_2O_3 peak at 35°) to facilitate comparison of the primary Rh peak at 41.2°. Panel C contains the full patterns for both monolith catalysts, fresh and used, staggered relative to one another by 10% of the maximum height. Panels A and B contain patterns for crushed Rh (fresh and used) and Rh-Ce (fresh and used) catalysts respectively. Results in Panel A indicate an increase in Rh crystallinity, suggesting an increase in crystallite size and therefore particle size. Results in Panel B indicate no change in Rh crystallinity between fresh and used catalysts with Ce.

4. UoMn – Understanding of inorganic impurities on catalytic performance

4.1 Experimental setup at University of Minnesota

Steam methane reforming (SMR) was chosen as a model system to study the effect of inorganics on rhodium catalysts. Methane shows negligible homogeneous chemistry at typical temperatures in a gasifier (500-1000 ˚C)[14]. Also, SMR is kinetically limited[15], hence the activity of the catalyst can be directly related to the conversion of methane. By performing SMR over undoped and inorganic-doped rhodium catalysts, the effect of inorganics on the rhodium sites involved in reforming to produce syngas can be studied.

Experimental setup

SMR was carried out in a quartz reactor (20 mm I.D.) over 3 g of 2.5 wt% Rh supported on 1.3 mm diameter α-Al_2O_3 spheres. A blank 80 ppi α-Al_2O_3 monolith (17 mm diameter, 10 mm long) was used to support the catalyst bed (Figure 32 (A) inset). Two blank 45 ppi α-Al_2O_3 monoliths were placed about 1 cm upstream of the 80 ppi monolith which acted as static mixers. The monoliths were held against the reactor walls by wrapping them with aluminosilicate cloth. Mass flow controllers regulated the flow rate of gases (N_2, H_2, CH_4) to the reactor, accurate to within ± 2%. Water was fed using a liquid handling pump through a heated coil maintained at approximately 200 °C to generate steam. A type-K thermocouple was placed between the two 45 ppi monoliths and a benchtop temperature controller (Omega CSC 32) controlled the temperature between the monoliths to within ± 1 °C. The reactor tube was placed in a furnace. Reforming being an endothermic process, this arrangement helped to insulate the reactor from the heat effects of the reaction.

Product analysis

Products were analyzed with an Agilent 6890 Gas Chromatograph equipped with a 30 m Plot-Q column and both thermal conductivity and flame ionization detectors. Water was quantified by closing the hydrogen and oxygen balances and averaging the two results. During operation, the carbon, hydrogen and oxygen balances generally closed to within ± 5%.

Selectivities to CO and CO_2 were calculated on a carbon basis and to H_2 and H_2O were on a hydrogen basis. Selectivity to a product is defined as (atoms in product species)/(atoms in converted fuel). Steam fed to the reactor was not considered fuel. The sum of selectivities to products on carbon or hydrogen basis was 100%, within the limits of experimental error.

Catalyst preparation

Catalysts used in all the experiments were 2.5 wt% Rh on α-Al_2O_3 spheres (1.3 mm diameter, Saint Gobain Norpro). Catalysts were prepared by the incipient wetness technique[16]. Rhodium nitrate solution (Sigma-Aldrich) was used as the rhodium precursor. Catalysts were dried, then calcined in a furnace at 800 °C for 6 h.

Experimental procedure

Each catalyst was initially aged at 850 °C for 3 h in a mixture of 20% steam, 10% methane and 70% nitrogen at a total flow rate of 2 SLPM. Subsequently, the temperature was reduced to 700 °C and the performance of the catalyst for SMR was measured. The residence time within the catalyst bed was approximately 20 ms at 700 °C. The inorganic species of interest was added to the catalyst (one inorganic atom for every five rhodium atoms) through its precursor by the incipient wetness technique and its performance was compared with the undoped catalyst at 700 °C.

Catalyst characterization

SEM images were taken on JEOL 6700 equipped with a secondary electron detector. Most samples were coated with 100 Å of carbon to reduce charging effects.

XRD was carried out on a Bruker D 5005 diffractometer equipped with a 2.2 kW sealed Cu source. Spheres were crushed to a fine powder increasing the peak intensities during analysis.

XPS studies were carried out on Surface Science SSX 100 with a monochromatic Al K-α source (1486.6 eV). The spot size used in the measurements corresponded to 800 µm. All peaks were calibrated with respect to the C 1s peak at 285 eV.

H_2 pulsed chemisorption was carried out by injecting pulses of hydrogen from a 5% hydrogen in argon mixture into a quartz tube containing 0.2 g of the catalyst sample. 15 pulses were injected into the catalyst at 1 minute intervals at 25 °C with a dwell time of 15 s. The outlet was connected to a thermal conductivity detector.

4.2 Performance testing results and discussion

The effect of inorganics on rhodium was studied by measuring the reactor performance for 5 h and through characterization by H_2 chemisorption, SEM, XPS and XRD before and after doping with inorganics.

All of the undoped catalysts showed similar baseline performance with about 67% methane conversion. Hydrogen and carbon monoxide selectivities were about 68% and 49% respectively. These parameters were used as an indicator of reactor performance and plotted with time for each inorganic during the 5 h operation period. The changes in conversions and selectivities are expressed in terms of the absolute difference between the average doped (over 5 h) and undoped values. For example, if the conversion decreased from 60% to 30%, this is equivalent to (60-30) = 30% and not 50% decrease in conversion.

Sulfur

Dimethyl sulfoxide was used to add sulfur to the catalyst. Sulfur decreased the methane conversion the most among all the inorganics studied. However, partial regeneration of the catalytic activity was observed during the 5h test period. Methane conversion (Figure 32 (A)) and hydrogen selectivity increased (Figure 32 (B)) with time from 19% and 32% respectively at the beginning to 31% and 42% at the end of 5 h. The CO selectivity increased by about 10% and was almost constant throughout the 5h duration (Figure 32 (B)).

Phosphorus

Ammonium phosphate was used as a precursor for introducing phosphorus to the catalyst. Phosphorus decreased the methane conversion by about 17% (Figure 32 (C)). Also, CO selectivity increased by 22% whereas H_2 selectivity decreased by 13% (Figure 32 (D)). After the 5 h performance testing period, a significant fraction of the spheres appeared black due to coke formation.

Silicon

Tetraethylorthosilicate (TEOS) was added to the aged rhodium catalyst to introduce silicon. The changes in methane conversion and product selectivities (not shown) were within the limits of experimental error.

Sodium and Potassium

Acetate precursors were used to add sodium and potassium to the catalyst. Sodium and potassium decreased methane conversions by 9% and 16%, respectively (Figure 33 (A) and (C)). Potassium decreased the H_2 and CO selectivities by 5% and 7% respectively, whereas the decrease with sodium was within experimental error as shown in Figure 33 (B) and (D).

Calcium and Magnesium

Calcium acetate and magnesium acetate tetrahydrate were used as calcium and magnesium precursors. Conversions and syngas selectivities were unchanged within limits of experimental error for both calcium and magnesium (not shown).

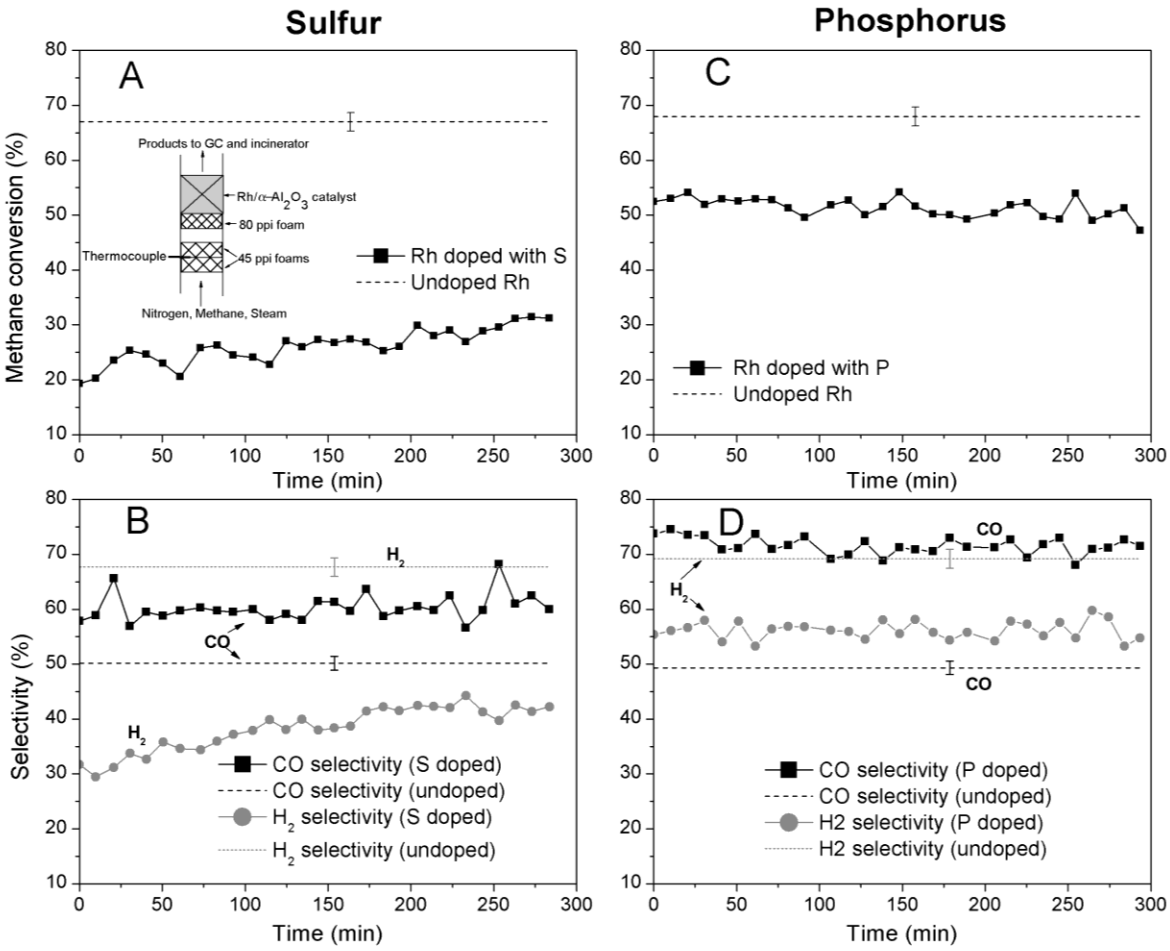

Figure 32 Methane conversion for catalysts doped with sulfur (A) and phosphorus (B) respectively. Hydrogen, carbon monoxide selectivities for catalysts doped with sulfur (C) and phosphorus (D) respectively. Figure 32 (A) also shows a schematic of the reactor setup.

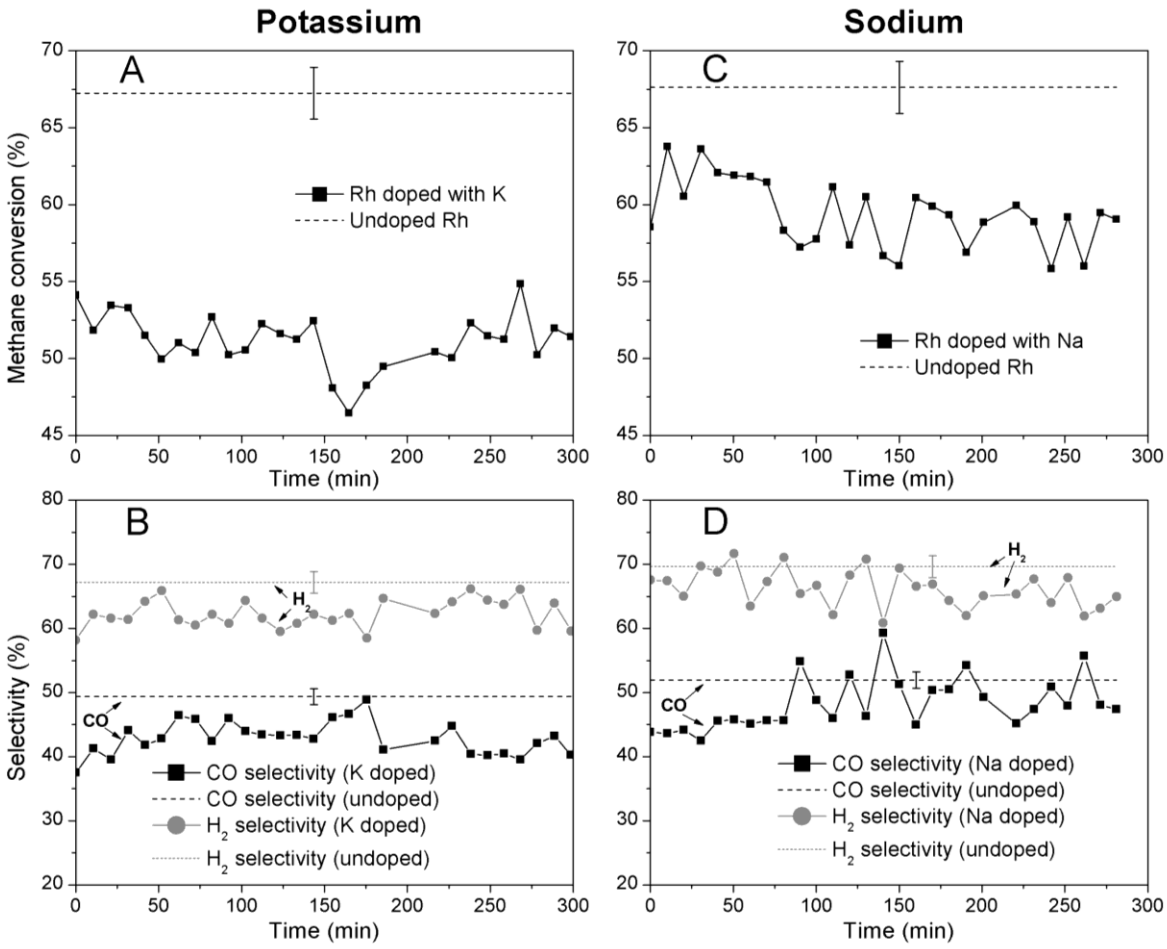

Figure 33 Methane conversion for catalysts doped with potassium (A) and sodium (B) respectively. Hydrogen, carbon monoxide selectivities for catalysts doped with potassium (C) and sodium (D) respectively.

The results of performance testing are summarized in Table 8.

Table 8 Change in methane conversion at 700 ˚C upon doping with different inorganics (1 atom inorganic/ 5 atoms of rhodium) as compared to aged undoped catalyst (2.5 wt% Rh/ α-Al_2O_3).

Inorganic	$-\Delta X_{CH4}$ (%)	ΔX_{CO} (%)	ΔX_{H2} (%)
S (t=0)	48	8	-36
S (t=5 h)	36	11	-26
P	17	22	-13
Si	~0	~0	~0
Na	9	~0	~0
K	16	-7	-5
Mg	~0	~0	~0
Ca	~0	~0	~0

4.3 Catalyst characterization of inorganics effects

4.3.1 H_2 chemisorption

The effect of the inorganics on the dispersion of rhodium on the α-Al_2O_3 support was analyzed by H_2 pulsed chemisorption. All the aged rhodium catalysts had a rhodium dispersion of approximately 10%. Phosphorus and sulfur decreased the dispersion of the catalyst (10.7% to 3.6% for phosphorus, 9.5% to 4.4% for sulfur). For the other inorganics, the change in dispersion was within the limits of experimental error.

4.3.2 SEM

Images were taken for each of the catalysts studied. Fresh, aged and Na, Ca, Mg, Si, and S doped catalysts appeared similar in terms of morphology, each showing particles around 50 nm in diameter (Figure 34 (A). Carbon formation was observed on the surface of catalysts doped with phosphorus and potassium. In the case of phosphorus-doped catalyst, the carbon formed was filamentous (Figure 34 (B)) with rhodium particles at the tips (Figure 34 (C)), whereas the carbon formed with potassium-doped catalyst showed the presence of needle-like structures (Figure 34 (D)). After placing the phosphorus-doped catalyst in a furnace at 500 °C for 30 min, the filamentous carbon on the catalyst was almost completely eliminated. The carbon on the potassium-doped catalyst remained even on heating at 750 °C for 30 min.

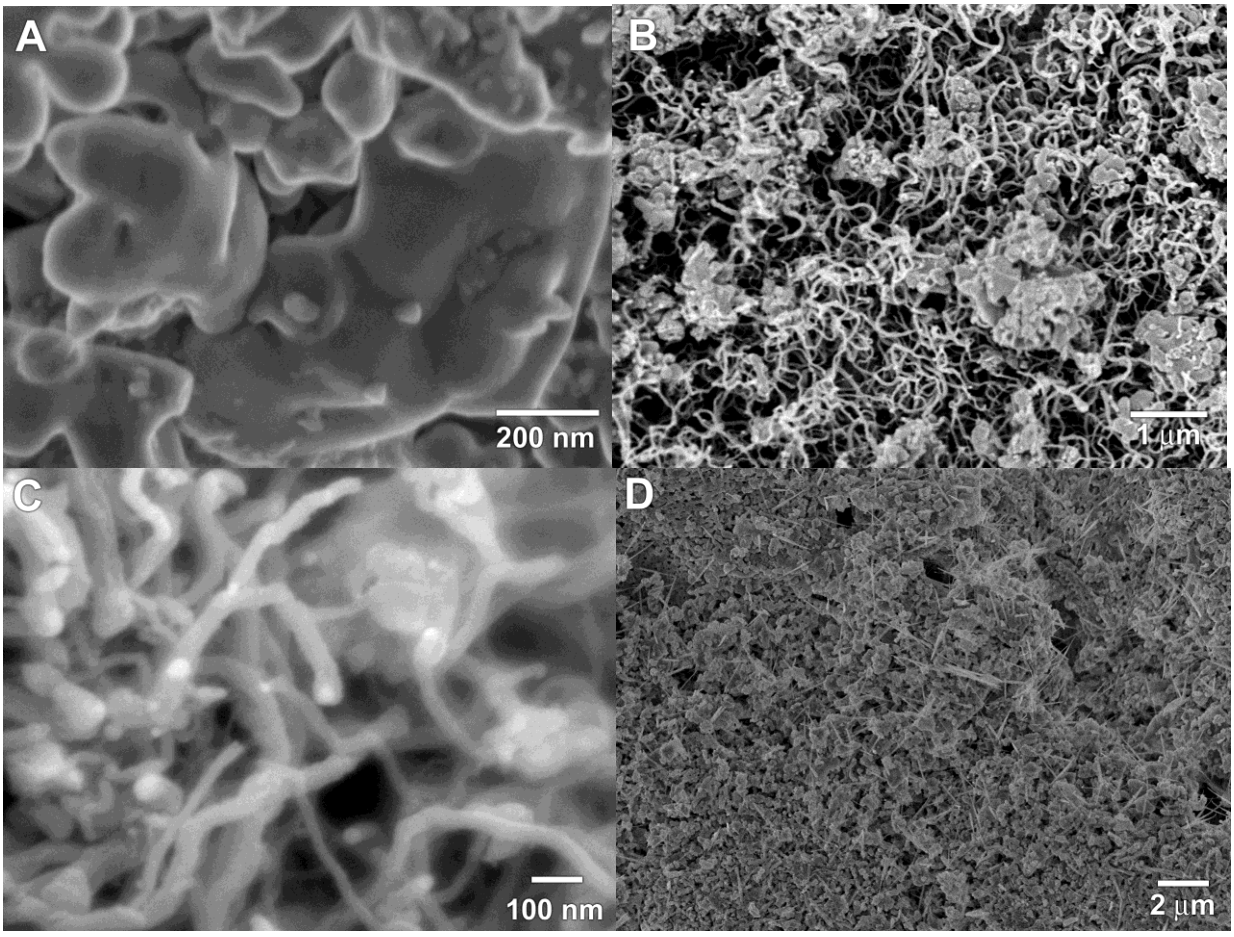

Figure 34 SEM images of (a) fresh 2.5 wt% Rh on α-Al_2O_3 catalyst (b) carbon filaments on catalyst doped with phosphorus (c) high resolution image of carbon filaments in catalyst doped

with phosphorus showing rhodium particles at tip and (d) carbon structures on catalyst doped with potassium.

4.3.3 XPS

The electronic interactions of the inorganics with rhodium were analyzed by XPS. The aging process decreased the rhodium binding energies of $3d_{5/2}$ and $3d_{3/2}$ peaks by about 1 eV showing conversion of rhodium oxide (Rh_2O_3, Rh^{+3}) to rhodium metal (Rh^0). Sodium, calcium, magnesium and silicon lowered the binding energy of rhodium by about 0.3 eV, whereas potassium decreased it by about 0.6 eV compared to the aged rhodium catalyst. Sulfur addition caused no change whereas phosphorus increased the rhodium binding energies compared to the aged rhodium catalyst by approximately 0.6 eV.

4.3.4 XRD

To examine the possibility of formation of any crystallites, XRD studies were performed. During the aging process, XRD analysis showed that all the rhodium oxide was converted into rhodium metal. No additional peaks were observed upon doping with inorganics. With phosphorus, additional small peaks were observed at 33 and 47 degrees corresponding to Rh_2P, rhodium phosphide.

4.3.5 Equilibrium calculations

The primary reactions in SMR are:

Steam reforming: $CH_4 + H_2O \leftrightarrow 3H_2 + CO$ (1)

Water gas shift: $CO + H_2O \leftrightarrow H_2 + CO_2$ (2)

Equilibrium calculations were performed to study the effect of the inorganics on the equilibrium of steam reforming (1) and water gas shift (2). The equilibrium constant for (1) and (2) at 700 °C was 12.1 and 1.6 respectively[17]. The experimental value of the proportionality constant for reactions (1) and (2) was calculated by the following equations:

$$K_{exp,SMR} = \frac{P_{H_2}^3 P_{CO}}{P_{H_2O} P_{CH_4}}$$ for steam reforming and

$$K_{exp,WGS} = \frac{P_{H_2} P_{CO_2}}{P_{H_2O} P_{CO}}$$ for water gas shift.

For the undoped rhodium catalysts, equilibrium analysis indicated that methane steam reforming is not equilibrated, whereas the water gas shift reaction reached equilibrium ($K_{exp,WGS} / K_{eq,WGS}$ ≈1) showing SMR is kinetically limited by (1).

Even upon addition of inorganics, water gas shift reaction was equilibrated for calcium, magnesium, sodium, potassium and silicon as the ratio $K_{exp,WGS} / K_{eq,WGS}$ was approximately 1. Doping with sulfur and phosphorus prevented the water gas shift reaction from proceeding to equilibrium as this ratio was about 0.3 and 0.25 respectively, showing the poisoning effect of sulfur and phosphorus on water gas shift activity.

5. GE-Kinetic modeling of biomass gasification tar removal

5.1 Summary of literature findings

Tars are the condensable organic fractions formed during biomass gasification. Tar is a complex mixture of heavy hydrocarbons and includes single ring to 5-ring aromatic compounds along with other oxygen-containing hydrocarbons and complex polycyclic aromatic hydrocarbon (PAH). Tars can be decomposed through cracking, steam and dry reforming reactions. [18]

Cracking: $pC_nH_x \rightarrow qC_mH_y + rH_2$

Steam reforming: $C_nH_x + nH_2O \rightarrow (n+x/2)H_2 + nCO$

Dry reforming: $C_nH_x + nCO_2 \rightarrow (x/2)H_2 + 2nCO$

Carbon formation: $C_nH_x \rightarrow nC+(x/2)H_2$

C_nH_x represents tar, and C_mH_y represents hydrocarbon with smaller carbon number than C_nH_x.

Due to the variety of compounds present in tars and the complexity of reactions involved in the tar conversion process, reaction mechanism and kinetic modeling for the tar removal system is not an easy task. As reviewed by Li et al.[18], most researchers studied tar elimination mechanisms by selecting model compounds. Typical model tar compounds are toluene, naphthalene, benzene, etc. Some other researchers adopt a global mechanism approach by considering all tar compounds as only one group. Those tars were assumed to disappear by several simultaneous reactions such as steam-, dry-, hydro- and thermal-reforming, cracking, etc. As shown in Figure 35, all tar compounds were lumped into one simple reaction network. The overall tar disappearance rate was calculated by summing the rate of all the elementary individual reactions.

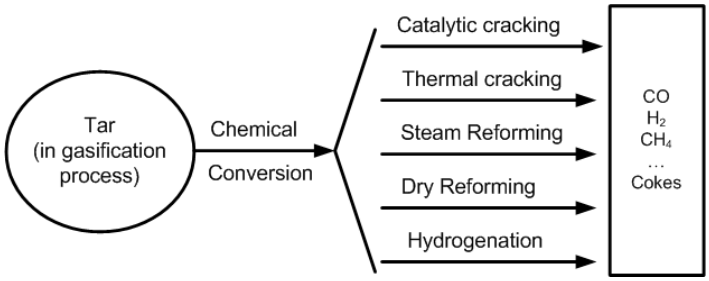

Figure 35 One-lump model used for tar elimination from biomass gasification[3]

The general reaction kinetic equations used by most researchers in the tar removal kinetics field are shown in the following.

$$-r_{tar} = k_{app} C_{tar}, \qquad k_{app} = k_{0,app} e^{(-\frac{E_{app}}{RT})}$$

$$k_{app} = \frac{-\ln(1-X)}{\tau}, \qquad \tau = \frac{W}{v_0}$$

Researchers used model compounds and derived reactant orders and kinetic parameters based on the equations shown above. A few selected kinetic data will be included in this report and will be used to compare with the model results that we have developed under this program.

Table 9 Kinetic data of thermal conversion of naphthalene, toluene and benzene

Hydrocarbon	Pre-exponential factor	Activation energy (kJ mol^{-1})	Reaction order		
			Hydrocarbon	Hydrogen	Steam
Naphthalene	$1.7 \times 10^{14}\ m^{0.3}\ mol^{-0.1}\ s^{-1}$	350	1.6	−0.5	0
Toluene	$3.3 \times 10^{10}\ m^{1.5}\ s^{-1}$	247	1[a]	0.5	0[a]
Benzene	$2.0 \times 10^{16}\ mol^{0.1}\ m^{-0.3}\ s^{-1}$	443	1.3	−0.4	0.2

[a] Assumption of first-order reaction with respect to toluene and zero-order reaction with respect to steam.

Table 10 Estimates of the kinetic parameters for the first-order toluene decomposition rate on Ni/olivine catalyst

Parameter	Estimated value
$k'(T_r)$ (m^3 (kg_{cat} h)$^{-1}$)	1896 (800 °C)
$A(k')$ (m^3 (kg_{cat} h)$^{-1}$)	3.14×10^{13}
E_a (kJ mol^{-1})	196

Table 11 Values for the apparent activation energy and pre-exponential factor for the overall tar removal reaction

	Commercial nickel-based catalyst (tar generated in a gasifier with air)	Over a calcined dolomite (tar generated in a gasifier with steam (Delgado et al. [37]))	Tar generated in a gasifier with air (Narvaez et al., 1996; [36])
$E_{app.}$(kJ mol^{-1})	72 ± 12	84 ± 6	97 ± 14
$k_{app.}$(m^3(NC) dry/(kg/h))	143,000	2600 ± 700	$(1.2–1.4) \times 10^6$

Table 9 is from Jess' kinetic calculations on thermal reactions of aromatic hydrocarbons[19]. Swierczynski et al.[20, 21] use toluene as model component of tar and conducted experiments in a laboratory scale fixed bed reactor. The reactor was considered as plug flow without gas expansion (constant flow rate). Tar decomposition rate was assumed to be first-order in their calculations and results are shown in Table 10[20, 21]. Table 11 shows kinetic data for different operating conditions in Narvaez et al.'s work[22]. In their work, a simple kinetic model is used to describe the overall tar elimination network. Corella et al.[23, 24] conducted extensive studies on tar elimination reactions and kinetics. Figure 36 is a summary of E_{app} values found by several authors with different catalysts. This serves as very useful references for researchers in this area.

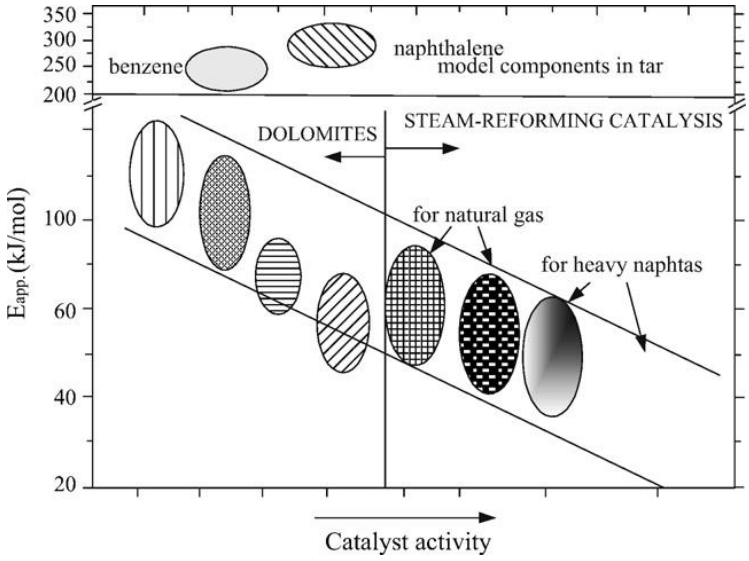

Figure 36 E_{app} values for first-order reaction of tar elimination over calcined dolomites and steam-reforming (nickel-based) catalysts

5.2 Reaction scheme and kinetic modeling from FCL work

Under this program, GE Fuel Conversion Laboratory and University of Minnesota have evaluated different tar components (benzene, toluene, methyl-naphthalene), with different reforming agents (steam, steam-air mixtures, steam-air-syngas mixtures) at different operating conditions. Figure 37 is a tar elimination reaction network that we proposed using toluene as the model tar compound. In this reaction network, a simulated biomass gasification producer gas containing syngas and tar was used. Additional air and steam were injected to the reactor for the tar reforming reaction. The feed mixture containing CO, H_2, O_2, H_2O, CO_2, N_2 and toluene was sent to a preheated Rh-Ce-Al_2O_3 catalyst. The preheat temperature is typically in the range of 300-500^oC, which is too low for the steam reforming of toluene to take place. It is speculated that, H_2 in the syngas, upon contact with the catalyst surface, first reacts with O_2 and releases a large amount of heat in a short time. This results in a rapid increase in surface temperature. The high temperature triggers the reforming reaction as shown in Step III in Figure 37. Water-gas shift reaction takes place as well to adjust the H_2/CO ratio in the product.

(I) Adsorption of toluene and gases on metal surfaces

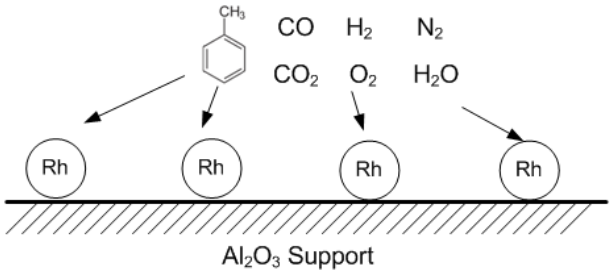

(II) Reaction of H_2 and O_2 on catalyst surface and a rapid surface temperature increase

$$H_2 + 0.5O_2 \rightarrow H_2O \qquad \Delta H_{298}=-242kJ/mol$$

(III) Reaction of toluene radicals at high temperatures and water-gas shift reaction

$$C_7H_8 \text{ (toluene)} + 7H_2O \rightarrow 7CO + 11H_2 \qquad \Delta H_{900}=-876kJ/mol$$

$$CO + H_2O \rightarrow CO_2 + H_2 \qquad \Delta H_{900}=-33kJ/mol$$

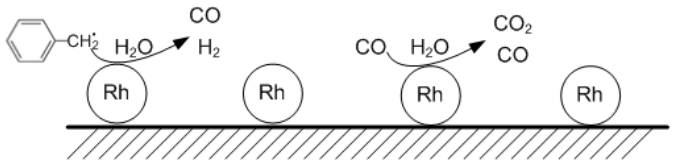

Figure 37 Proposed tar conversion reaction scheme with air and steam in the gas phase

5.3 Kinetic modeling results and discussion

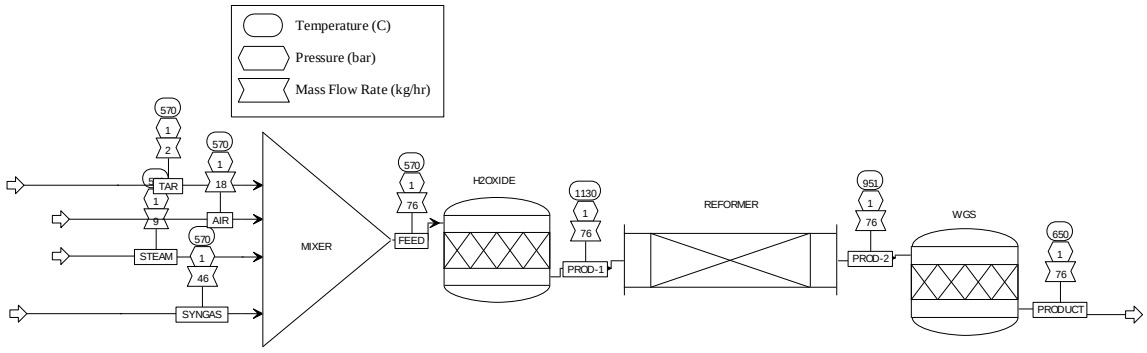

Figure 38 Catalytic tar removal process simulation model in AspenPlus^{TM}

Figure 38 shows a process simulation model we built using AspenPlus^{TM} to study tar removal kinetics. This process was designed with the guidance of the tar removal reaction pathway proposed in Figure 37. It is speculated that, H_2 in the syngas, upon contact with the catalyst surface, first reacts with O_2 and releases a large amount of heat in a short time. A rapid

increase in surface temperature triggers the tar steam reforming reaction, which is the primary route for removal of tar from the feed. Additionally, water-gas shift reaction takes place to adjust the H_2/CO ratio in the product. As presented in Figure 38, a H_2 oxidizer was included to simulate the reaction between H_2 in the syngas and O_2 in the air. The mixture stream eluting out from the H_2 oxidizer, at a dramatically higher temperature and with O_2 eliminated, was sent to the tar reformer. All the tar removal takes place in this reactor. A WGS reactor was included downstream of the reformer to further adjust product distribution between H_2, CO and CO_2.

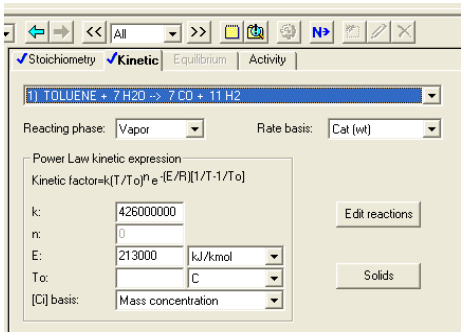

Figure 39 Tar reforming kinetic reaction in the plug flow reformer

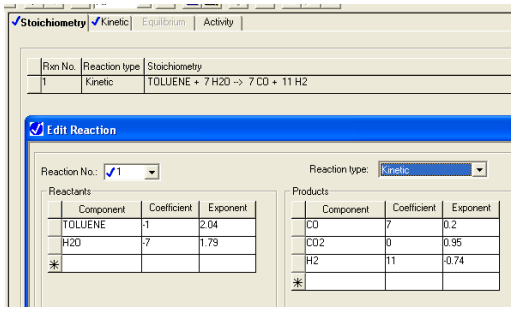

Figure 40 Tar reforming reaction orders in the plug flow reformer

In the AspenPlus model (Figure 38), the H_2 oxidizer assumes 100% conversion of O_2. The subsequent reformer is an adiabatic plug flow reactor. The tar steam reforming reaction kinetic (in our example, toluene) was built into the reactor (shown in Figure 39). The activation energy used in Figure 39 was decided based on literature search presented in the previous quarterly report. The reaction orders shown in Figure 40 were obtained from literature[25]. The WGS reactor is modeled as an Equilibrium reactor.

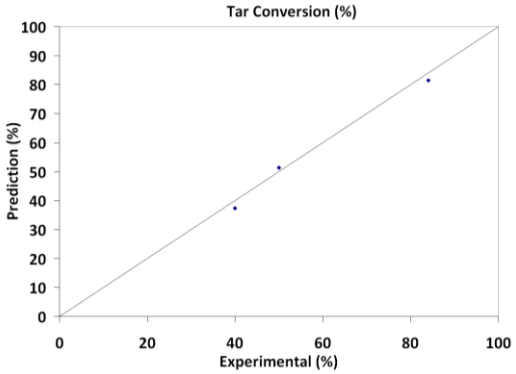

(a)

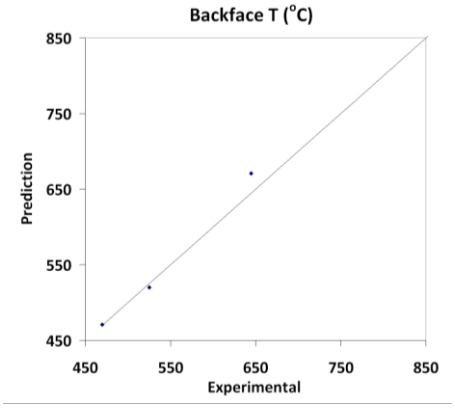

(b)

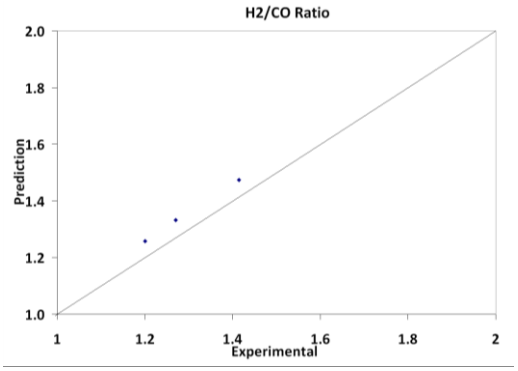

(c)

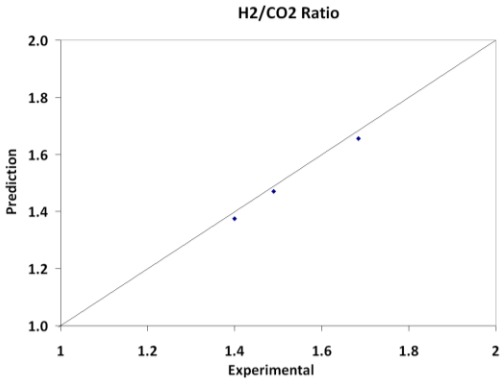

(d)

Figure 41 Comparison between modeled data and experimental data: (a) Tar conversion; (b) Catalyst backface temperature; (c) H_2/CO ratio in product; (d) H_2/CO_2 ratio in product

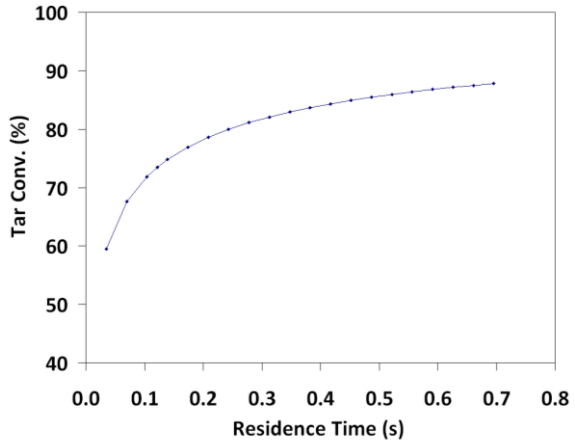

Figure 42 Modeled tar conversion as a function of residence time (S/C=3, O/C=1.5, preheat T=500^{o}C)

Experimental data (eg. tar conversion, reactor inlet and outlet temperatures, product distribution) at different operating conditions were used to validate the model. Figure 41 shows comparisons between modeled data and experimental data. A good fit between model predictions and experimental data was found for operating conditions within the range of interest for this program: O/C <=1.5, S/C <=3, inlet T <=500^{o}C. Parameters for the components in the model need to be refined to achieve a good fit if operating conditions fall out of this range. This is expected due to changes in heat duty and reaction equilibrium when operating conditions vary significantly. This model will be a valuable tool in designing the tar removal reactor and identifying appropriate operating conditions. As an example, Figure 42 plotted modeled tar removal performance as a function of residence time in the reactor using the model. Depending on the gasifier type and tar removal requirements, reactor dimension and catalyst specification can be estimated based on data presented in Figure 42.

Reference

1. Milne, T. A. and Evans, R. J., Biomass Gasifier "Tars": Their Nature, Formation, and Conversion *National Renewable Energy Laboratory Report: NREL/TP-570-25357* **1998**.
2. Coll, R., Salvadó, J., Farriol, X. and Montané, D., Steam reforming model compounds of biomass gasification tars: conversion at different operating conditions and tendency towards coke formation *Fuel Process. Technol.* **2001,** 74 (1), 19.
3. Hohn, K. L. and Schmidt, L. D., Partial oxidation of methane to syngas at high space velocities over Rh-coated spheres *Appl. Catal. A: Gen* **2001,** 211 (1), 53.
4. Corella, J., Orio, A. and Aznar, P., Biomass Gasification with Air in Fluidized Bed: Reforming of the Gas Composition with Commercial Steam Reforming Catalysts *Ind. Eng. Chem. Res.* **1998,** 37 (12), 4617.
5. Turn, S. Q., Kinoshita, C. M., Ishimura, D. M., Hiraki, T. T., Zhou, J. and Masutani, S. M., An Experimental Investigation of Alkali Removal from Biomass Producer Gas Using a Fixed Bed of Solid Sorbent *Ind. Eng. Chem. Res.* **2001,** 40 (8), 1960.
6. Horn, R., Williams, K. A., Degenstein, N. J., Bitsch-Larsen, A., Dalle Nogare, D., Tupy, S. A. and Schmidt, L. D., Methane catalytic partial oxidation on autothermal Rh and Pt foam catalysts: Oxidation and reforming zones, transport effects, and approach to thermodynamic equilibrium *J. Catal.* **2007,** 249 (2), 380.
7. Colby, J. L., Wang, T. and Schmidt, L. D., Steam Reforming of Benzene As a Model for Biomass-Derived Syngas Tars over Rh-Based Catalysts *Energ. Fuel* **2009,** 24 (2), 1341.
8. Delahay, G., Ensuque, E., Coq, B. and Figuéras, F., Selective Catalytic Reduction of Nitric Oxide byn-Decane on Cu/Sulfated-Zirconia Catalysts in Oxygen Rich Atmosphere: Effect of Sulfur and Copper Contents *J. Catal.* **1998,** 175 (1), 7.
9. Church, J. S., Cant, N. W. and Trimm, D. L., Stabilisation of aluminas by rare earth and alkaline earth ions *Appl. Catal. A: Gen* **1993,** 101 (1), 105.
10. Trovarelli, A., Catalytic Properties of Ceria and CeO2-Containing Materials *Catalysis Reviews: Science and Engineering* **1996,** 38 (4), 439.
11. Simell, P. A., Hepola, J. O. and Krause, A. O. I., Effects of gasification gas components on tar and ammonia decomposition over hot gas cleanup catalysts *Fuel* **1997,** 76 (12), 1117.
12. Donazzi, A., Beretta, A., Groppi, G. and Forzatti, P., Catalytic partial oxidation of methane over a 4% Rh/[alpha]-Al2O3 catalyst Part II: Role of CO2 reforming *J. Catal.* **2008,** 255 (2), 259.
13. Rajvanshi, A. K., Alternative Energy in Agriculture; CRC Press **1986,** 2, 83.
14. Jones, G., Jakobsen, J. G., Shim, S. S., Kleis, J., Andersson, M. P., Rossmeisl, J., Abild-Pedersen, F., Bligaard, T., Helveg, S., Hinnemann, B., Rostrup-Nielsen, J. R., Chorkendorff, I., Sehested, J. and Nørskov, J. K., First principles calculations and experimental insight into methane steam reforming over transition metal catalysts *J. Catal.* **2008,** 259 (1), 147.
15. Bizzi, M., Basini, L., Saracco, G. and Specchia, V., Short contact time catalytic partial oxidation of methane: analysis of transport phenomena effects *Chem. Eng. J.* **2002,** 90 (1-2), 97.
16. Colby, J. L., Dauenhauer, P. J. and Schmidt, L. D., Millisecond autothermal steam reforming of cellulose for synthetic biofuels by reactive flash volatilization *Green Chem.* **2008,** 10 (7), 773.
17. Choi, Y. and Stenger, H. G., Water gas shift reaction kinetics and reactor modeling for fuel cell grade hydrogen *J. Power Sources* **2003,** 124 (2), 432.
18. Li, C. and Suzuki, K., Tar property, analysis, reforming mechanism and model for biomass gasification--An overview *Renew. Sust. Energ. Rev.* **2009,** 13 (3), 594.

19. Jess, A., Mechanisms and kinetics of thermal reactions of aromatic hydrocarbons from pyrolysis of solid fuels *Fuel* **1996,** 75 (12), 1441.
20. Swierczynski, D., Courson, C. and Kiennemann, A., Study of steam reforming of toluene used as model compound of tar produced by biomass gasification *Chem. Eng. Process.* **2008,** 47 (3), 508.
21. Swierczynski, D., Libs, S., Courson, C. and Kiennemann, A., Steam reforming of tar from a biomass gasification process over Ni/olivine catalyst using toluene as a model compound *Appl. Catal. B: Environ* **2007,** 74 (3-4), 211.
22. Narvaez, I., Orio, A., Aznar, M. P. and Corella, J., Biomass Gasification with Air in an Atmospheric Bubbling Fluidized Bed. Effect of Six Operational Variables on the Quality of the Produced Raw Gas *Ind. Eng. Chem. Res.* **1996,** 35 (7), 2110.
23. Corella, J., Toledo, J. M. and Aznar, M.-P., Improving the Modeling of the Kinetics of the Catalytic Tar Elimination in Biomass Gasification *Ind. Eng. Chem. Res.* **2002,** 41 (14), 3351.
24. Corella, J., Caballero, M. A., Aznar, M.-P. and Brage, C., Two Advanced Models for the Kinetics of the Variation of the Tar Composition in Its Catalytic Elimination in Biomass Gasification *Ind. Eng. Chem. Res.* **2003,** 42 (13), 3001.
25. Devi, L., Ptasinski, K. J. and Janssen, F. J. J. G., Decomposition of Naphthalene as a Biomass Tar over Pretreated Olivine:â€‰ Effect of Gas Composition, Kinetic Approach, and Reaction Scheme *Ind. Eng. Chem. Res.* **2005,** 44 (24), 9096.